

# Higgs production in association with squark pairs in the Minimal Supersymmetric Standard Model at future hadron colliders

A. Dedes and S. Moretti

*Rutherford Appleton Laboratory, Chilton, Didcot, Oxon OX11 0QX, UK*

## Abstract

We study neutral and charged Higgs boson production in association with stop and sbottom squarks at the Large Hadron Collider, within the Supergravity inspired Minimal Supersymmetric Standard Model. The phenomenological relevance of such reactions is twofold. Firstly, they constitute a novel production mechanism of Higgs particles, either through a decay of a heavier (anti)squark into a lighter one or via a Higgs bremsstrahlung process. Secondly, their production rates are extremely sensitive to the values assumed by the five input parameters of the model, this possibly allowing one to put stringent constraints on the latter. After an exhaustive scan of the parameter space, we find that the majority of such processes could be detectable at high luminosity, provided  $\tan\beta$  is large,  $\tan\beta \gtrsim 30$  (except in the case of  $\tilde{t}_1\tilde{t}_1^*h$  and  $\tilde{t}_1\tilde{t}_2^*h$  final states, whose detection is also possible for smaller values), that the universal soft Supersymmetric breaking masses are in the ranges  $M_0 \lesssim 500$  GeV and  $M_{1/2} \lesssim 220$  GeV, and that the trilinear couplings are negative,  $A_0 < 0$ . We also point out some sizable decay signatures and discuss their Standard Model (SM) backgrounds. Finally, we derive compact analytical formulae of the corresponding scattering matrix elements.

# 1 Introduction and motivation

‘If Supersymmetry (SUSY) exists, it will be discovered at the next generation of hadronic machines’, has been a recurring motto so far. Indeed sooner (at the Tevatron,  $\sqrt{s} = 2$  TeV) or later (at the Large Hadron Collider (LHC),  $\sqrt{s} = 14$  TeV), depending on the mass scale of the Higgs bosons and of the Superpartners of ordinary matter, several Supersymmetric ‘signatures’ should clearly be viable<sup>1</sup>. Typical SUSY events at hadron colliders will involve either the production and decay of heavy spartons, squarks and gluinos, whose foreseen mass range is expected to be around the TeV scale [3], or of Higgs bosons [4], primarily of the lightest one, for which the SUSY theory imposes a stringent mass bound of the order of the electroweak (EW) scale.

However, even assuming that such a discovery will take place, there might well be little to learn about the fundamental dynamics of SUSY from such new events. In fact, although, e.g., the LHC is able to produce gluinos and squarks with masses up to 2 TeV or so and their detection has been shown to be feasible with rather little effort [5], it is much more difficult to determine exactly the SUSY masses involved, because in most models (i.e., those assuming  $R$ -parity conservation) there are at least two missing SUSY particles in each event. Clearly, failing the knowledge of the SUSY mass spectrum, other typical SUSY quantities, such as couplings, decay rates, etc., cannot be assessed either. Needless to say, their measurement would be of paramount importance in order to constrain the free parameters entering the SUSY Lagrangian. However, by resorting to specific kinematic distributions [5], it is at least possible to make precision measurements of some ‘combinations’ of SUSY masses, but only in a few fortunate cases these can lead to strong constraints on the theory and its parameters. Besides, in minimal SUSY theories, the Higgs sector typically (i.e., at tree level) depends on only two such parameters, the ratio of the vacuum expectation values (VEVs) of the Higgs fields and one of the masses of the five physical states corresponding to the latter, as all others SUSY inputs enter through higher perturbative orders. Therefore, even the detection of a SUSY Higgs signal would carry very poor information in terms of the underlying SUSY model. As a matter of fact, a second question about SUSY has to legitimately be risen. Namely, ‘Which Supersymmetric model will one discover?’

Thus, the key task for the Tevatron and the LHC is not only to find SUSY, but also to assess which model is behind it and the value of its parameters. For example, in the context of Supergravity (SUGRA) inspired models [6], with the minimal particle content of the MSSM (henceforth denoted as M-SUGRA, that we take to be the reference framework of our analysis) [7, 8], the dynamics of the theory can be specified by only five entries: (i) a universal scalar mass  $M_0$ ; (ii) similarly, that for the gauginos  $M_{1/2}$ ; (iii) the universal trilinear breaking terms  $A_0$  (all defined at the Grand Unification scale  $M_{\text{GUT}}$  [9]). After the radiative EW symmetry breaking has taken place, two further parameters are needed to describe the low energy dynamics: (iv) the mentioned ratio of the VEVs of the two Higgs fields, denoted by  $\tan\beta \equiv v/v'$  and defined at the EW scale; and (v) a discrete parameter,  $\text{sign}(\mu) = \pm 1$ , being  $\mu$  the Higgsino mass term.

Assuming universal soft breaking terms at the GUT scale, one is then able to calculate

---

<sup>1</sup>For some reviews, see, e.g., [1] and [2].

the masses of SUSY (s)particles, their couplings, decay rates, etc., at the EW scale, through the evolution of the renormalisation group equations (RGEs), the latter involving  $M_0$ ,  $M_{1/2}$ ,  $A_0$ ,  $\tan\beta$  and  $\text{sign}(\mu)$  as inputs. Ultimately, a comparison of such predictions with the corresponding experimental measurements, as reconstructed from the actual data via dedicated Monte Carlo (MC) simulations [10]–[12], should allow one to impose indirect constraints on the above parameters. Indeed, an additional procedure to follow in order to determine the latter could well be to search for the evidence of some more exotic signals of SUSY, in which, however, the dependence on such parameters is somewhat more manifest.

Elementary processes of the type

$$g + g \longrightarrow \tilde{q}_\chi + \tilde{q}_{\chi'}^* + \Phi, \quad (1)$$

where  $q^{(\prime)} = t, b$ ,  $\chi^{(\prime)} = 1, 2$  and  $\Phi = H, h, A, H^\pm$ , in all possible combinations, as appropriate in the MSSM, serve the double purposes of:

1. furnishing production mechanisms of Higgs bosons of the MSSM, both neutral and charged, in addition to the Standard Model (SM)-like channels [4];
2. yielding production rates, for particular combinations of  $q^{(\prime)}$ ,  $\chi^{(\prime)}$  and  $\Phi$ , strongly dependent on some of the fundamental SUSY parameters of the M-SUGRA model.

The importance of the first point should be understood in the following terms. On the one hand, the detection of all neutral Higgs particles  $H$ ,  $h$  and  $A$  of the theory is not certain, neither at the Tevatron [1] nor even at the LHC [2]. In addition, the discovery potential of heavy charged Higgs bosons  $H^\pm$  at both the above colliders has been proved to be extremely limited [13]. Under these circumstances, the possible existence of novel and detectable Higgs production channels represents a phenomenologically important result per se. (Notice that, for certain choices of  $\text{sign}(\mu)$ ,  $A_0$  and  $\tan\beta$ , the squark-squark-Higgs coupling can become the largest EW coupling of the SUSY theory, even exceeding the standard Yukawa ones.) On the other hand, the fact that in processes (1) the Higgs bosons are produced in association with squarks via a Yukawa bremsstrahlung or in ‘non-dominant’ squarks decays<sup>2</sup>, implies that the Higgs mechanism can be probed in the sparticle sector too. In fact, other known production and decay mechanisms used to detect MSSM Higgs bosons mainly involve Higgs couplings to ordinary matter. The only exceptions are the squark loop-contributions to neutral Higgs boson production via gluon-gluon fusion and to Higgs boson decays through pairs of photons/gluons [14], which are however swamped in both modes by the dominant terms involving ordinary heavy particles.

As for the second point that we put forward, we should remind the reader of the actual form of the mentioned squark-squark-Higgs vertices in the MSSM (which can be found, e.g., in [15]). In many of these, namely when  $\chi \neq \chi'$ , both the low-energy SUSY parameters  $\mu$  and  $\tan\beta$  enter explicitly in the Feynman rules, other than implicitly in the scalar masses. Furthermore, those vertices also contain  $A_{q^{(\prime)}}$ , the trilinear couplings at the EW scale, which

---

<sup>2</sup>So that the corresponding partial widths are significantly different from the total widths, thus retaining the dynamics of the squark-squark-Higgs production vertices also at decay level.

depend critically on their common value at the GUT scale,  $A_0$ . (In the case  $\Phi = A$  such a dependence is also not affected by the mixing between the chiral,  $\chi^{(\prime)} = L, R$ , and physical,  $\chi^{(\prime)} = 1, 2$ , squark states, so that no additional SUSY mixing parameters enter the phenomenology of pseudoscalar Higgs production, this rendering the latter an ideal laboratory to study M-SUGRA effects [16]). Therefore, one should expect a significant dependence of the production rates of the scattering processes (1) on  $\tan\beta$ ,  $A_0$  and  $\mu$  (particularly, its sign), this possibly yielding a new profitable mean to constrain the underlying SUSY model. Even more so in the case  $\tan\beta$  has previously been determined, for example, through a discovery in the MSSM Higgs sector.

Concerning previous literature on the subject, we should mention that reactions of the type (1) were first considered in Ref. [17] for the case  $gg \rightarrow \tilde{t}_1 \tilde{t}_1^* h$  in the so-called ‘decoupling’ limit. Adopting the M-SUGRA scenario, associated production of both neutral and charged Higgs bosons production with squark pairs – with a special emphasis on CP-odd Higgs boson production – was first considered by the authors in [16]. Furthermore, in Ref. [18] (and also [19]) light Higgs boson production in association with light top squarks was reanalysed in the M-SUGRA scenario at both Tevatron and LHC<sup>3</sup>. A general consensus on the possible detectability at the LHC of  $gg \rightarrow \tilde{t}_1 \tilde{t}_1^* h$  events emerged from Refs. [17, 18, 19], in the case of light top squarks and large trilinear coupling.

We generalise here those studies, as we consider the production of all possible Higgs states,  $\Phi = H, h, A$  and  $H^\pm$ , for a broader spectrum of their masses, in conjunction with both squark flavours that can have sizable couplings to Higgs particles,  $\tilde{q} = \tilde{t}$  and  $\tilde{b}$ , the latter taken as not degenerate in mass, also allowing for Higgs production in decay channels, when  $\chi \neq \chi'$ . On the other hand, to simplify the simulation, we restrict ourselves to the case of gluon-gluon induced processes only, thus neglecting the case of quark-antiquark scatterings, which was instead considered in Refs. [17, 18]. This is however not restrictive. In fact, we have verified that at the LHC the  $gg$  contribution is around two order of magnitudes larger than the  $Q\bar{Q}$  one, in line with the findings of Refs. [17, 18], well below the level of uncertainties arising in our computation from other sources (such as structure functions, QCD  $K$ -factors, etc.)<sup>4</sup>. As for the Tevatron, we can anticipate that the production cross sections of processes (1) are generally very small (see also Ref. [18]), indeed below the level of detection over most of the M-SUGRA parameter space, so that we neglect further consideration of this machine here.

It is the purpose in this paper to assess the possible relevance of points 1. and 2. in phenomenological studies of SUSY to be carried out at the LHC. In particular, the plan of the paper is as follows. In the next Section we describe how we have proceeded in our calculations. In Sect. 3 we illustrate the theoretical model we have resorted to in our analysis. Sect. 4 presents some numerical results. A brief summary and our conclusions are given in Sect. 5. Finally, we collect in Appendix the relevant analytical formulae that we have used.

---

<sup>3</sup>The same final state but produced in  $e^+e^-$  annihilations at the TeV scale, e.g., at the Next Linear Collider, has been considered in Refs. [18, 20].

<sup>4</sup>As for  $\gamma, Z$  and  $W^\pm$   $s$ -channels, these are typically smaller by a factor of the order  $\mathcal{O}(\alpha_{\text{em}}/\alpha_s)^2$ ; whereas  $\mathcal{O}(\alpha_s)^2$  gluino interactions in  $t, u$ -channels are suppressed by the small (EW induced) mixing between light quarks and sbottom and stop squarks, as already remarked in [17].

## 2 Calculation

The leading-order (LO) Feynman diagrams associated to processes of the type (1) in the unitary gauge are depicted in Fig. 1. The reader can find an analytical expression of the corresponding matrix elements (MEs) in the Appendix. As a test of the correctness of our amplitudes, we have verified that they are gauge invariant by checking various Ward identities of the theory, both analytically and numerically. The amplitudes squared have then been integrated over a three-body phase space, using VEGAS [22], and convoluted with gluon Parton Distribution Functions (PDFs), as provided by CTEQ(4L) [23]. The latter constitutes our default set, taken at LO in order to be consistent with our approximation in calculating the scattering MEs. However, in order to estimate the systematic error due to the gluon behaviour inside the proton, we also have resorted to other LO packages, such as MRS-LO(09A,10A,01A,07A) [24]. Typical differences among PDFs were found to be less than 15–20%. The centre-of-mass (CM) energy at the partonic level,  $Q = \sqrt{\hat{s}}$ , was the scale used to evaluate both the structure functions and the strong coupling constant (see next Section for the treatment of the latter).

Depending on the relative value of the final state masses in (1),  $m_{\tilde{q}_X}$ ,  $m_{\tilde{q}'^*_X}$  and  $m_\Phi$ , the production of Higgs particles can be regarded as taking place either via a (anti)squark decay (if  $m_{\tilde{q}_X} > m_{\tilde{q}'^*_X} + m_\Phi$  or  $m_{\tilde{q}'^*_X} > m_{\tilde{q}_X} + m_\Phi$ ) or via a Higgs-strahlung (if  $m_{\tilde{q}_X} < m_{\tilde{q}'^*_X} + m_\Phi$  and  $m_{\tilde{q}'^*_X} < m_{\tilde{q}_X} + m_\Phi$ ). In the first case, to prevent our MEs from becoming singular, we need to insert a finite width in the resonant (anti)squark propagators, which we have done by adopting the Breit-Wigner expression given in the Appendix and the appropriate numerical values for the widths, calculated as described in Sect. 3. Also in the second case, though no poles exist in the amplitudes, a finite width value has been retained in the propagators. Notice that we have treated the two processes on the same footing, without making any attempt to separate them, as for the time being we are only interested in the total production rates of the  $2 \rightarrow 3$  processes (1), rather than in their subsequent decay distributions.

## 3 The theoretical model and its parameters

In this paper we are going to display our results for squark-squark-Higgs production via processes (1) by assuming possibly the simplest scenario in the choice of the soft SUSY breaking parameters at the GUT scale. That is, the so-called minimal Supergravity scenario or M-SUGRA inspired model, as already intimated in the Introduction. In this scenario, the whole dynamics of the MSSM (which contains over hundred parameters in the case of conserved  $R$ -parity) at the GUT scale is reduced to the three basic inputs already introduced:  $M_0$ ,  $M_{1/2}$  and  $A_0$ . The large top Yukawa coupling then triggers the radiative EW breaking through the running of the soft Higgs breaking masses, from the GUT scale down to EW regime. From the minimisation conditions of the potential one can define the soft Higgs mixing parameter,  $B$ , and the absolute value of the Higgs mixing parameter of the SUSY potential,  $\mu$ . The model leaves the  $\text{sign}(\mu)$  and the value of  $\tan\beta$  as further undetermined

parameters at the EW scale.

All five M-SUGRA parameters enter into the relevant Feynman rules for the squark-squark-Higgs vertices, either explicitly or implicitly (through the RGEs). These can be written in the physical squark basis  $\tilde{q}_{1,2}$  as

$$\begin{aligned}
\lambda_{\Phi\tilde{q}_1\tilde{q}'_1} &= c_q c_{q'} \lambda_{\Phi\tilde{q}_L\tilde{q}'_L} + s_q s_{q'} \lambda_{\Phi\tilde{q}_R\tilde{q}'_R} + c_q s_{q'} \lambda_{\Phi\tilde{q}_L\tilde{q}'_R} + s_q c_{q'} \lambda_{\Phi\tilde{q}_R\tilde{q}'_L}, \\
\lambda_{\Phi\tilde{q}_2\tilde{q}'_2} &= s_q s_{q'} \lambda_{\Phi\tilde{q}_L\tilde{q}'_L} + c_q c_{q'} \lambda_{\Phi\tilde{q}_R\tilde{q}'_R} - s_q c_{q'} \lambda_{\Phi\tilde{q}_L\tilde{q}'_R} - c_q s_{q'} \lambda_{\Phi\tilde{q}_R\tilde{q}'_L}, \\
\lambda_{\Phi\tilde{q}_1\tilde{q}'_2} &= -c_q s_{q'} \lambda_{\Phi\tilde{q}_L\tilde{q}'_L} + s_q c_{q'} \lambda_{\Phi\tilde{q}_R\tilde{q}'_R} + c_q c_{q'} \lambda_{\Phi\tilde{q}_L\tilde{q}'_R} - s_q s_{q'} \lambda_{\Phi\tilde{q}_R\tilde{q}'_L}, \\
\lambda_{\Phi\tilde{q}_2\tilde{q}'_1} &= -s_q c_{q'} \lambda_{\Phi\tilde{q}_L\tilde{q}'_L} + c_q s_{q'} \lambda_{\Phi\tilde{q}_R\tilde{q}'_R} - s_q s_{q'} \lambda_{\Phi\tilde{q}_L\tilde{q}'_R} + c_q c_{q'} \lambda_{\Phi\tilde{q}_R\tilde{q}'_L},
\end{aligned} \tag{2}$$

where  $\tilde{q}_{L,R}$  or  $\tilde{q}'_{L,R}$  can in principle be any flavour of chiral squarks. However, here we only focus our attention to the case of the third generation of down and up squarks only, namely, sbottom and stop scalars, whose physical mass eigenstates are denoted by  $\tilde{b}_{1,2}$  and  $\tilde{t}_{1,2}$ , respectively, the subscript 1(2) referring to the lightest(heaviest) of them. As usual, the Higgs fields are denoted by the generic symbol  $\Phi$ , where  $\Phi = H, h, A, H^\pm$ . All the  $\lambda_{\Phi\tilde{q}_x\tilde{q}'_{x'}}$ 's appearing in eq. (2) are function of  $\mu, \tan\beta$  and  $A_{t,b}$  and can be read directly from the Appendix of Ref. [15]. (We ignore the case of complex  $\mu$  and  $A_q$  ( $q = t, b$ ) parameters by assuming that their phases are very small, the preferred case following the measurements of the Electric Dipole Moments [25].)

Also the left-right squark mixing angles  $s_q \equiv \sin\theta_q$  and  $c_q \equiv \cos\theta_q$  (here,  $q = t, b$ ) depend on the M-SUGRA parameters, since they read as

$$\begin{aligned}
\tan(2\theta_t) &= \frac{2m_t(A_t - \mu \cot\beta)}{M_{\tilde{Q}_3}^2 - M_{\tilde{U}_3}^2 + (\frac{1}{2} - \frac{4s_W^2}{3})M_Z^2 \cos 2\beta}, \\
\tan(2\theta_b) &= \frac{2m_b(A_b - \mu \tan\beta)}{M_{\tilde{Q}_3}^2 - M_{\tilde{D}_3}^2 + (-\frac{1}{2} + \frac{2s_W^2}{3})M_Z^2 \cos 2\beta},
\end{aligned} \tag{3}$$

with  $M_Z$  the  $Z$ -boson mass and  $s_W \equiv \sin^2\theta_W$  the sine (squared) of the Weinberg angle,  $m_t$  and  $m_b$  the top and bottom quark masses, where  $A_t$  and  $A_b$  are the trilinear couplings defined at the EW scale, while  $M_{\tilde{Q}_3}$ ,  $M_{\tilde{U}_3}$  and  $M_{\tilde{D}_3}$  are the running soft SUSY breaking squark masses of the third generation, for which we assume the values obtained from their evolution starting from a universal mass at the GUT scale equal to  $M_0$ .

Regarding the numerical values of the M-SUGRA parameters adopted in this paper, we have proceeded as follows. For a start, we have set  $M_0 = M_{1/2} = 150$  GeV. Such rather low values for the universal masses come as natural first choice, if one is interested in detecting processes of the type (1). For two simple reasons. On the one hand, these two quantities determine the actual  $m_{\tilde{q}_x}$ ,  $m_{\tilde{q}'_{x'}}$  and  $m_\Phi$  values entering processes (1), through their intervention in the RGEs, in such a way that small values of  $M_0$  and  $M_{1/2}$  at the GUT scale convert into a rather light squark and Higgs mass spectrum at the EW scale. On the other hand, being  $2 \rightarrow 3$  body processes, a strong suppression from the phase space would arise

in squark-squark-Higgs production if the masses in the final state were too large<sup>5</sup>. For the above choice, the M-SUGRA model predicts squark and heavy Higgs masses in the region of 80–450 GeV (as we shall see in more detail below), so that the latter can in principle materialise at LHC energies (further recall that the light Higgs mass is bound to be below 130 GeV).

Then, we have varied the trilinear soft Supersymmetry breaking parameter  $A_0$  in a region where it changes its sign, e.g.,  $(-300, +300)$  GeV, while we spanned the  $\tan\beta$  value between 2 and 40. As for  $\mu$ , whereas in our model its magnitude is constrained, its sign is not. Thus, in all generality, we have explored both the possibilities  $\text{sign}(\mu) = \pm 1$ .

As a further step of our analysis, we have then come back to  $M_0$  and  $M_{1/2}$  and change them, while maintaining  $\tan\beta$ ,  $A_0$  and  $\text{sign}(\mu)$  fixed at some specific values. We have done so only for those processes that we had already identified to have not only a large cross section, but also a strong dependence on one or more of these three M-SUGRA parameters.

Given the strong phase space suppression induced by the consequent increase of  $m_{\tilde{q}_\chi}$ ,  $m_{\tilde{q}'_\chi}$  and  $m_\Phi$  in the final states, we will cautiously maintain the universal scalar and gaugino masses below 250–300 GeV (at least at first). However, the reader should not assume that this is a necessary condition to the experimental detection of processes of the type (1). In fact, this need not be true, as we shall show that even for  $M_0$  values as large as 500 GeV one can find sizable squark-squark-Higgs production cross sections for  $M_{1/2}$  up to 200–250 GeV, as long as  $A_0$  is strongly negative,  $\tan\beta \gtrsim 30$  and  $\text{sign}(\mu) < 0$ .

Such unexpected behaviours are strongly driven by the intervention in the production rates of  $\tan\beta$ ,  $A_0$  and  $\text{sign}(\mu)$ , through the trilinear scalar couplings  $\lambda_{\Phi\tilde{q}_\chi\tilde{q}'_\chi}$ , more than by the actual values of  $m_{\tilde{q}_\chi}$ ,  $m_{\tilde{q}'_\chi}$  and  $m_\Phi$ . This is evident by a mere look at the standard Feynman rules, as can be found, e.g., in Ref. [15]. We will make our concern in this paper that of guiding the reader through such delicate interplay between masses and couplings, by explicitly writing down the expression of the relevant vertices in those parameter space domains where such complicated phenomenology manifests itself.

Starting from the five M-SUGRA parameters  $M_0$ ,  $M_{1/2}$ ,  $A_0$ ,  $\tan\beta$  and  $\text{sign}(\mu)$ , we have generated the spectrum of masses, widths, couplings and mixings relative to squarks and Higgs particles entering reactions (1) by running the **ISASUGRA/ISASUSY** programs contained in the latest release of the package **ISAJET** [10], version 7.40. The default value of the top mass we used was 175 GeV. Note that also typical EW parameters, such as  $\alpha_{\text{em}}$  and  $\sin^2\theta_W$ , were taken from this program, as they enter the RGEs of the SUSY theory. Concerning the value of the strong coupling constant,  $\alpha_s$ , entering the production processes (1), we have proceeded as follows. By using as inputs the extracted value of  $\alpha_s$  at the  $M_Z$  scale, we evolve it up to any scale  $Q$  by making use of the two-loop renormalisation group equations and by taking into account all the low-energy threshold effects from the various SUSY masses by means of the theta function approximation, as discussed in Ref. [26].

---

<sup>5</sup>The additional depletion coming from the gluon PDFs, which would be probed at much higher values of  $Q^2$  (of the order of the rest masses or more), where they are naturally smaller, would in part be compensated by the rise of the quark-antiquark initiated subprocesses: i.e.,  $Q + \bar{Q} \rightarrow \tilde{q}_\chi + \tilde{q}'_\chi + \Phi$ , where, again, one has that  $q^{(\prime)} = t, b$ ,  $\chi^{(\prime)} = 1, 2$  and  $\Phi = H, h, A, H^\pm$ .

Finally, notice that in scanning over the M-SUGRA parameter space, one should make sure that the values generated for the Higgs boson and sparticle masses are in accordance with current experimental bounds. Signs of the sort “ $\times$ ” or shaded areas appearing in our figures in forthcoming Sect. 4 will correspond to already prohibited areas for the parameter space of our SUSY model. We nonetheless leave them for illustrative purposes, in order to visualise the typical impact of present and future experimental bounds on the phenomenology of our reactions. For example, the M-SUGRA points individuated by the combinations  $M_0 = M_{1/2} = 130 - 150$  GeV,  $\tan \beta = 2$ ,  $A_0 = 0$  GeV and  $\text{sign}(\mu) = -$ , used in some of the tables and figures in the next Section, contradict the limits on the lightest Higgs boson mass from direct searches [27, 28], as they yield  $m_h = 72 - 80$  GeV. We will discuss the experimental bounds in more detail in the next Section.

As for theoretical constraints, these arise from two sources: namely, the absence of charge and colour breaking minima and that of large contributions to the EW observables that are measured with high precision at LEP. The former is avoided when the following inequalities hold tree level [29]:

$$\begin{aligned} A_t^2 &< 3 \left( m_{\tilde{Q}_3}^2 + m_{\tilde{U}_3^c}^2 + \mu^2 + m_{H_2}^2 \right), \\ A_b^2 &< 3 \left( m_{\tilde{Q}_3}^2 + m_{\tilde{D}_3^c}^2 + \mu^2 + m_{H_1}^2 \right), \\ A_\tau^2 &< 3 \left( m_{\tilde{L}_3}^2 + m_{\tilde{E}_3^c}^2 + \mu^2 + m_{H_1}^2 \right), \end{aligned} \tag{4}$$

where all masses appearing in eq. (4) are the soft Supersymmetry breaking masses except the Higgsino mixing parameter  $\mu$ . When  $A_0$  is below 1 TeV, as is the case in our analysis, the above constraints are always satisfied even for very light squark masses. As for the contributions to the EW observables, we have found the region  $150 \text{ GeV} \lesssim M_0, M_{1/2} \lesssim 500$  GeV,  $2 \lesssim \tan \beta \lesssim 40$  and  $|A_0| \lesssim 900$  GeV covered by our analysis in agreement with the most recent measurements of the ‘effective’ weak mixing angle,  $\sin^2 \theta_{\text{eff}} = 0.2321 \pm 0.010$ , and of the  $W^\pm$  mass,  $M_W = 80.388 \pm 0.063$  GeV [30]. In particular, notice that the M-SUGRA prediction for  $\sin^2 \theta_{\text{eff}}$  decreases for a lighter mass spectrum while it becomes constant in the heavy mass region [31].

## 4 Results

We begin this Section by analysing all reactions (1) in the low mass regime, i.e., that induced by values of  $M_0$  and  $M_{1/2}$  below 250–300 GeV. This is done in Subsect. 4.1. In this scenario, we will first present and discuss, for future reference, the values of squark and Higgs masses resulting from the RGE evolution: in 4.1.1 and 4.1.2, respectively. Then, we will move on to considering the production of, in turn: neutral CP-even (in 4.1.3), CP-odd (in 4.1.4) and charged (in 4.1.5) Higgs bosons. Possible decay signatures of the latter will be analysed in 4.1.6. Finally, Subsect. 4.2 will pin-point those unusual cases discussed above, in which the suppression from very heavy scalar masses in the final states of reactions (1) can be overcome by strong vertex effects, yielding in the end sizable cross sections.



## 4.1 Light mass spectrum

Once fixed  $M_0 = M_{1/2} = 150$  GeV, one obtains the (sbottom and stop) squark and Higgs masses reported in Figs. 2 and 3, respectively, depending on  $2 \lesssim \tan \beta \lesssim 35$  and for  $A_0 = -300, 0, +300$  GeV. The two possible options for the sign of  $\mu$  are also contemplated.

Far from willing to discuss exhaustively the dependence of  $m_{\tilde{q}_\chi}$ ,  $m_{\tilde{q}'_\chi}$ , and  $m_\Phi$  upon the five M-SUGRA parameters, we limit ourselves here to spotting in Figs. 2–3 some interesting trends, that will affect the overall behaviour of the squark-squark-Higgs cross sections that we will be treating below. For a more complete overview, see, e.g., Refs. [32].

### 4.1.1 Squark masses

The four squark flavours of the first and second generation ( $\tilde{q} = \tilde{u}, \tilde{d}, \tilde{c}, \tilde{s}$ ) with left- and right-handed components are all nearly degenerate in mass and the latter is given approximately by the following formula:

$$m_{\tilde{q}} \simeq \sqrt{M_0^2 + 6M_{1/2}^2}, \quad (\tilde{q} = \tilde{u}, \tilde{d}, \tilde{c}, \tilde{s}). \quad (5)$$

For our choice of  $M_0$  and  $M_{1/2}$ , one gets  $m_{\tilde{q}} \simeq 400$  GeV. The light squark flavours are not our concern in processes (1), though they may well enter some of the decay chains of the other (pseudo)scalar particles produced.

The two squark flavours of the third generation must be treated differently because the off-diagonal entries of their mass matrices can be large, owing to the strength of the Yukawa couplings of the corresponding quarks (in this respect, notice that the bottom one becomes comparable to that of the top in the large  $\tan \beta$  region [15]). It thus follows that the mass eigenstates  $\tilde{t}_1, \tilde{t}_2, \tilde{b}_1$  and  $\tilde{b}_2$  are all different and generally smaller than  $m_{\tilde{q}}$ . Among these,  $\tilde{t}_1$  is most often significantly lighter than all the other stop and sbottom states. At large  $\tan \beta$ , the same happens to the  $\tilde{b}_1$  mass eigenstate, as large values of  $\tan \beta$  correspond to smaller sbottom masses, so that one eventually gets that  $m_{\tilde{t}_1} \simeq m_{\tilde{b}_1}$ .

Variation of the trilinear couplings can also cause significant differences between the light stop and sbottom masses. Finally, the sign of the Higgsino mass term plays an important rôle when  $\tan \beta$  is either small or large, for the cases  $m_{\tilde{t}_{1,2}}$  and  $m_{\tilde{b}_{1,2}}$ , respectively.

Experimental limits on the squark masses come from searches at Tevatron and LEP2. The most stringent bound on the  $\tilde{t}_1$  mass comes from the hadron collider [35]: in absence of mixing, values of  $m_{\tilde{t}_1} < 120$  GeV are excluded for<sup>6</sup>  $m_{\text{LSP}} \equiv m_{\tilde{\chi}_1^0} < 38$  GeV. DØ exclude values of  $m_{\tilde{b}_1}$  below 85 GeV for  $m_{\tilde{\chi}_1^0} < 47$  GeV [33] and ALEPH do over the region  $m_{\tilde{b}_1} < 83$  GeV for any value of LSP mass [34]. In addition, CDF exclude masses for the lightest top squark up to 120 GeV when the LSP is  $m_{\tilde{\chi}_1^0} < 50$  GeV [35]. Finally, DØ, using data corresponding to an integrated luminosity of 79 pb<sup>-1</sup>, contradicts all models with  $m_{\tilde{q} \neq \tilde{t}_1, \tilde{b}_1} < 250$  GeV for  $\tan \beta \lesssim 2$ ,  $A_0 = 0$  GeV and  $\mu < 0$  [36] (in scenarios with equal squark and gluino masses the limit goes up to  $m_{\tilde{q} \neq \tilde{t}_1, \tilde{b}_1} < 260$  GeV).

<sup>6</sup>Recall that in M-SUGRA the Lightest Supersymmetric Particle (LSP) is the lightest neutralino,  $\tilde{\chi}_1^0$ .

### 4.1.2 Higgs boson masses

The mass of the lightest Higgs boson is here constrained to be less than 115 GeV and it appears to exhibit constant values over the region  $8 \lesssim \tan \beta \lesssim 35$ , for a given combination of  $A_0$  and  $\text{sign}(\mu)$ . To change either the trilinear coupling or the sign of the Higgsino mass has the net effect of scaling  $m_h$ , lower with increasing  $A_0$  and higher for positive  $\mu$ .

As for the masses of the other Higgs bosons, they are nearly degenerate. They vary between 180 GeV (when  $\tan \beta$  is large) and 400 GeV (when  $\tan \beta$  is small). The dependence on  $\text{sign}(\mu)$  is generally negligible, whereas the one on  $A_0$  is very strong in the intermediate  $\tan \beta$  regime. One thing worth noticing here is the existence of a point where all three Higgs masses  $m_H, m_A$  and  $m_{H^\pm}$  converge, regardless of the values of  $A_0$  and  $\text{sign}(\mu)$ . This occurs for  $\tan \beta \approx 30$ , where

$$m_H = m_A = m_{H^\pm} \approx 200 \text{ GeV}. \quad (6)$$

As for experimental bounds, LEP experiments have combined their results from data taken at CM energies from 91 to 183 GeV to place lower bounds on the masses of the light ( $m_h$ ) and pseudoscalar ( $m_A$ ) Higgs bosons, of 78.8 and 79.1 GeV, respectively [37]. In addition, they exclude the range  $0.8 < \tan \beta < 2.1$  for minimal stop mixing and  $m_t = 175$  GeV. Also, DØ [38] have recently removed at 95% confidence level the intervals  $\tan \beta < 0.97$  and  $\tan \beta > 40.9$  for  $M_{H^\pm} = 60$  GeV and  $\sigma(t\bar{t}) = 5.5$  pb (again, with  $m_t = 175$  GeV). However, the limits become less stringent with increasing  $M_{H^\pm}$ : e.g., for  $M_{H^\pm} > 124$  GeV (as is the case here) the available angular range is  $0.3 < \tan \beta < 150$ .

### 4.1.3 CP-even Higgs boson production

We present in Figs. 4–5 the  $\tan \beta$  dependence of the production cross sections of the two neutral scalar Higgs bosons,  $h$  and  $H$ , respectively, in association with any possible combination of squarks of the third generation. Again, we parametrise the dependence upon  $A_0$  by adopting for the latter the discrete values of  $-300, 0$  and  $+300$  GeV and we choose  $\text{sign}(\mu) = \pm 1$ .

Assuming an integrated luminosity of 100 inverse femtobarns over a twelve month period of running at the LHC (i.e.,  $\int \mathcal{L} dt = 100 \text{ fb}^{-1}$ ), one can realistically hope for the detection of squark-squark-Higgs processes only if the production cross section is above 1 fb or so. In fact, we shall see in Sect. 4.1.6 how typical decay fractions of clean signatures range at the level of 10% or below (see Subsect. 4.1.6 later on).

Under this assumption, one immediately sees that there are several production channels of CP-even Higgs particles which could be observed, over a large part of the M-SUGRA parameter space considered here. Primarily, those involving the lightest stop squark,  $\tilde{t}_1$ , particularly if also the lightest Higgs state is involved, but not only.

For the case of  $h$  production, there exists an approximate hierarchy of cross sections which can possibly be detected:

$$\sigma(\tilde{t}_1 \tilde{t}_1^* h) \gtrsim \sigma(\tilde{t}_1 \tilde{t}_2^* h) \gtrsim \sigma(\tilde{b}_1 \tilde{b}_1^* h). \quad (7)$$

The cases  $\tilde{b}_2 \tilde{b}_2^* h$ ,  $\tilde{t}_2 \tilde{t}_2^* h$  and  $\tilde{b}_1 \tilde{b}_2^* h$  never have significantly large rates.

In the case of  $\tilde{t}_1\tilde{t}_1^*h$  states, those with largest production rates, one obtains

$$\sigma(gg \rightarrow h\tilde{t}_1\tilde{t}_1^*) \gtrsim 20 \text{ fb}, \quad (8)$$

for every combination of  $\tan\beta$ ,  $A_0$  and  $\text{sign}(\mu)$ , in the case of  $M_0 = M_{1/2} = 150 \text{ GeV}$ , thus a sort a lower limit over a representative portion of the low mass regime of the M-SUGRA scenario. Moreover, the largest production rate for this final state (compatible with the current experimental constraints) is obtained in the small  $\tan\beta \sim 2$  region and for the combinations  $A_0 \lesssim -300$  and  $\mu = +$ , for which

$$\sigma(\tilde{t}_1\tilde{t}_1^*h) \gtrsim 200 \text{ fb}, \quad (9)$$

corresponding to more than 20000 events per year running of the LHC.

The dominance of the production channel involving both the lightest squarks and Higgs boson, above all other mechanisms (1), was foreseeable. The reason is rather simple, in fact, twofold. On the one hand, the sum of the rest masses in the final states yields the smallest possible values, thus enhancing the volume of the three-body phase space, relatively to any other squark-squark-Higgs combination. On the other hand, the cross section is also significantly enhanced when the trilinear coupling  $A_0$  assumes negative values. From the analysis of the RGEs we find that  $A_t \sim -400(-250) \text{ GeV}$  when  $A_0 = -300(300) \text{ GeV}$ . Now, the coupling of the light Higgs boson to top squarks is driven by  $A_t$  when the latter takes on large values. More specifically, the corresponding vertex reads as (recall that we are in the kinematic limit  $m_X \approx m_H \approx m_A \approx m_{H^\pm} \gg M_Z$ : see Fig. 3)

$$\begin{aligned} \lambda_{h\tilde{t}_1\tilde{t}_1^*}^{m_X \gg M_Z} &\simeq \frac{ig_W M_Z}{c_W} \left\{ \left[ -\frac{1}{2} \cos 2\beta \cos^2 \theta_{\tilde{t}} + \frac{2}{3} s_W^2 \cos 2\beta \cos 2\theta_{\tilde{t}} \right] \right. \\ &\quad \left. - \frac{m_{\tilde{t}}^2}{M_Z^2} - \frac{m_t \sin 2\theta_{\tilde{t}}}{2M_Z^2} (A_t + \mu \cot \beta) \right\}, \end{aligned} \quad (10)$$

(here and in the following,  $g_W^2 = 4\pi\alpha_{\text{em}}/s_W^2$ ,  $c_W = \sqrt{1 - s_W^2}$  and  $M_W^2 = M_Z^2(1 - s_W^2)$ ) where for large  $A_t$  (note that  $\sin \theta_{\tilde{t}}$  is maximal in such a case) the coupling goes like  $\lambda_{h\tilde{t}_1\tilde{t}_1^*} \propto \frac{m_t A_t}{M_Z^2}$ . As a consequence, because of the presence of the trilinear term  $A_t$ , the coupling of the light Higgs boson to light stop squarks could be much larger compared to that to the top quark, which behaves like  $\lambda_{htt} \propto \frac{m_t}{M_Z}$ , as already recognised in [17, 18]. Over the parameter space that we have chosen here, the cross section of  $gg \rightarrow \tilde{t}_1\tilde{t}_1^*h$  can be either larger than or of the same order as that of  $gg \rightarrow t\bar{t}h$  [17, 18].

Thus, the subprocess  $gg \rightarrow \tilde{t}_1\tilde{t}_1^*h$  can well boast the status of an additional discovery mechanism of the lightest scalar Higgs boson of the MSSM, as remarked in Refs. [17, 18]. (This is true also in non M-SUGRA models, where however one still has that  $m_H \approx m_A \approx m_{H^\pm} \gg m_h$  [17, 18].) In this respect, the reader should further notice the stability of its production cross section against variations of  $\tan\beta$  (see also, e.g., Fig. 4 in [18])<sup>7</sup>. This

---

<sup>7</sup>The  $\tan\beta$  dependence of  $\sigma(\tilde{t}_1\tilde{t}_1^*h)$  at low values of such a parameter is mainly a phase space effect, as it can be deduced by comparing Fig. 2 to Fig. 4. In addition, in the low  $\tan\beta$  domain, there are residual effects onto the production rates induced by the term  $\mu \cot\beta$  arising from the off-diagonal elements of the squark mass matrices and affecting the  $\lambda_{h\tilde{t}_1\tilde{t}_1^*}$  vertex.

proves to be a crucial point, as it is possible that one will have no narrow hints about the actual value of this crucial parameter of the Higgs sector even after Run 2 at Tevatron (unless, of course, the lightest Higgs boson is discovered there !) [35]. In other terms,  $\tilde{t}_1\tilde{t}_1^*h$  would always be present at fixed rate at the LHC, no matter whether  $\tan\beta$  is large or small. Similar arguments can be put forward concerning the  $\text{sign}(\mu)$  dependence.

Some care must instead be exercised with respect to the  $A_0$  dependence. In fact, to vary the universal trilinear coupling between, e.g.,  $-300$  and  $+300$  depletes the cross section by a factor of about seven, as shown in Fig. 4. For even larger differences, say, between  $-500$  and  $+500$  (not shown here for reasons of space), the ratio between the cross sections become as big as 30 ! Not surprisingly then, Ref. [18] focused on the choice  $A_0 = -2000$  GeV<sup>8</sup> (and  $\text{sign}(\mu) = +$ ). Far from regarding this dependence as a shortcoming of  $\tilde{t}_1\tilde{t}_1^*h$  events in helping in the quest for the so far elusive lightest Higgs boson of the MSSM (in fact, even for very large and positive  $A_0$  values we found the cross section well above 1 fb), this example allows us to enlighten that other aspect of squark-squark-Higgs production that we have mentioned in the Introduction: i.e., its potential in pinning down some of the fundamental parameters of the M-SUGRA model. Needless to say, variations of the cross section with  $A_0$  as large as those mentioned above are well beyond the various sources of uncertainties on the production rates (other than the theoretical ones related to the PDFs and the effect of higher-order QCD corrections also the experimental ones in their determination). To measure a production rate of  $\tilde{t}_1\tilde{t}_1^*h$  events much larger than about 50 fb (the value obtained in correspondence of  $A_0 = 0$ ), in some specific decay channel, would unambiguously imply that the universal trilinear coupling at the GUT scale is negative.

As already mentioned, very little could be learn about the actual values of  $\tan\beta$  from this specific process. However, if the latter is known beforehand to be around 2 or so, one could use this information to constrain  $\text{sign}(\mu)$ . In fact, for  $A_0 = -300$  GeV, one would get that

$$\sigma(\tilde{t}_1\tilde{t}_1^*h) \approx 200 \text{ fb} \Rightarrow \mu = + \quad (11)$$

$$\sigma(\tilde{t}_1\tilde{t}_1^*h) \approx 50 \text{ fb} \Rightarrow \mu = - . \quad (12)$$

Let us proceed in this spirit to see whether other channels can be of some help in constraining the M-SUGRA model. Following the list of detectable  $h$  production cross section given in (7), we find the  $\tilde{t}_1\tilde{t}_2^*h$  final state [16]. This is not surprising either. In fact, the relevant coupling behaves like (again,  $X = H, A, H^\pm$ )

$$\begin{aligned} \lambda_{h\tilde{t}_1\tilde{t}_2}^{m_X \gg M_Z} &\simeq \frac{ig_W M_Z}{c_W} \left\{ \frac{1}{2} \cos 2\beta \left( \frac{1}{2} - \frac{4}{3} s_W^2 \right) \sin 2\theta_{\tilde{t}} \right. \\ &\quad \left. - \frac{m_t \cos 2\theta_{\tilde{t}}}{2M_Z^2} (A_t + \mu \cot \beta) \right\} , \end{aligned} \quad (13)$$

becoming very large when  $\cos 2\theta_{\tilde{t}}$  and  $(A_t + \mu \cot \beta)$  reach their allowed maximum values.

---

<sup>8</sup>Note that in this  $A_0$  region the M-SUGRA scenario clashes against the constraints from the charge and colour breaking minima, i.e., eq. (4). This is the reason why we prefer to display our results in a rather more conservative range, i.e.,  $|A_0| \lesssim 1$  TeV.

From Fig. 4, one can see that this happens in the region of small  $\tan\beta$ , negative sign of  $\mu$  and  $A_0 \lesssim -300$  GeV.

The intriguing aspect here, which was largely missing in the case in which both squarks were the lightest, is that one could impose severe constraints on the sign of the Higgsino mass term, other than on  $A_0$ . In fact, in the detectable region, the curves corresponding to  $\text{sign}(\mu) = -$  (higher) and  $\text{sign}(\mu) = +$  (lower) depart considerably. For example, for relatively small  $\tan\beta$  values, say 4, the ratios as obtained by dividing the cross sections corresponding to negative  $\mu$ 's by those for positive Higgsino masses are quite large indeed: about 7(5)[2] when  $A_0 = -300(0)[+300]$  GeV. At even lower  $\tan\beta$ , say, equal to 2, one symbolically has:

$$\sigma(\tilde{t}_1\tilde{t}_2^*h) \approx 300 \text{ fb} \Rightarrow \mu = - \quad (14)$$

$$\sigma(\tilde{t}_1\tilde{t}_2^*h) \approx 2 \text{ fb} \Rightarrow \mu = + , \quad (15)$$

(e.g., for  $A_0 = -300$  GeV). Luckily enough here, where the solid and dot-dashed curves start getting closer (for  $\tan\beta \gtrsim 15 - 20$ ) is precisely when the cross section is no longer observable. However, what just said makes the point that  $\tan\beta$  ought to be known rather accurately from some previous measurements, if one wants to constrain the other M-SUGRA parameters by studying the production of the lightest Higgs scalar of the theory produced in association with both stop mass eigenstates.

In our list of observable  $h$  cross sections  $\tilde{b}_1\tilde{b}_1^*h$  comes next. Here the potential is somewhat complementary to the two above cases, in the sense that not to find any pairs of sbottom squarks of the type  $\tilde{b}_1$  produced in association with an  $h$  scalar once  $\tan\beta$  is already known to be large could have powerful consequences on the viability of M-SUGRA as the underlying model of SUSY. To be specific, notice how the six curves corresponding to all the possible combinations of the parameters  $A_0 = -300, 0, +300$  GeV and  $\text{sign}(\mu) = \pm$  lie within a factor from 2 to 4 in cross section, in correspondence of  $\tan\beta = 20$  and 35, respectively. Even the cases of  $A_0 = \pm 500$  GeV do not depart significantly from the central curve for  $A_0 = 0$ , in the above  $\tan\beta$  region. Unfortunately, contrary to the case of  $\tilde{t}_1\tilde{t}_2^*h$  production, here the most interesting region is presumably below detection level. In fact, for  $\tan\beta$  quite low, a huge portion of M-SUGRA parameter plane collapses into a narrow stripe, as the various curves tend to overlap, all being contained within a factor as small as 1.5 (e.g., at  $\tan\beta = 2$ , also including the cases  $|A_0| = 500$  GeV, not shown in the figure).

As for  $H$  production, one identifies as possible candidates for detection the following cases:

$$\sigma(\tilde{b}_1\tilde{b}_1^*H) \sim \sigma(\tilde{t}_1\tilde{t}_1^*H) \gtrsim \sigma(\tilde{b}_2\tilde{b}_2^*H) \sim \sigma(\tilde{t}_1\tilde{t}_2^*H). \quad (16)$$

The remaining two combinations, i.e.,  $\tilde{b}_1\tilde{b}_2^*H$  and  $\tilde{t}_2\tilde{t}_2^*H$ , yield cross sections that are hopelessly small.

Also some of the detectable  $H$  production processes can have a significant impact in aiding the determination of the M-SUGRA parameters, most notably those yielding the final states  $\tilde{b}_1\tilde{b}_1^*H$  and  $\tilde{b}_2\tilde{b}_2^*H$ . Here, if  $\tan\beta$  is known to be, say, 35 or so, a detection of either the former or the latter by the thousand or hundred, respectively, would imply that  $A_0$  is most certainly negative, since production rates corresponding to  $A_0$  values larger than

zero are about a factor of 5 and 3 smaller (rather irrespectively of  $\text{sign}(\mu)$ ). Somewhat less discrimination power between positive and negative  $A_0$  values have  $\tilde{t}_1\tilde{t}_1^*H$  and  $\tilde{t}_1\tilde{t}_2^*H$  events, over the same (large)  $\tan\beta$  region as above. The most interesting case would have been  $\tilde{t}_2\tilde{t}_2^*H$ , as the collapse of the M-SUGRA model that we already noticed in the case of  $\tilde{b}_1\tilde{b}_1^*h$  final states is here even more striking, over a more significant  $\tan\beta$  region. Unluckily enough, the corresponding production cross section never exceeds the femtobarn level.

A general remark is now in order, concerning the strength of the coupling of sbottom squarks to neutral CP-even Higgs bosons. The monotonic growth of the production rates of sbottom squark processes with increasing  $\tan\beta$ , as opposed to a much milder dependence of the stop ones, has a simple explanation. For example, the coupling  $\lambda_{h\tilde{b}_1\tilde{b}_1}$  is driven by the term  $\frac{m_b\mu\tan\beta}{M_Z^2}$  and its size becomes large for large  $\tan\beta$ . Another reason for an extra enhancement of the sbottom production rates comes from the phase space available to the final states, as both  $m_{\tilde{b}_1}$  and  $m_{\tilde{b}_2}$  decrease very fast when  $\tan\beta$  gets large, whereas this is much less the case for  $m_{\tilde{t}_1}$  and  $m_{\tilde{t}_2}$  (see Fig. 2). There is however a point, for the case of reactions involving the two sbottom mass eigenstates at once (i.e.,  $\tilde{b}_1\tilde{b}_2^*h$  and  $\tilde{b}_1\tilde{b}_2^*H$ ), in which the production cross sections vanish altogether, somewhere in the vicinity of  $\tan\beta = 34 - 36$  (the zero for  $\tilde{b}_1\tilde{b}_2^*H$  is actually beyond the  $\tan\beta$  range plotted), the exact value depending upon  $A_0$  and  $\text{sign}(\mu)$ . This is clearly induced by the  $\lambda_{h\tilde{b}_1\tilde{b}_2}$  and  $\lambda_{H\tilde{b}_1\tilde{b}_2}$  vertices and their typical  $\propto (\mu - A_b \tan\beta)$  behaviour, when  $|\mu| \ll |A_b \tan\beta|$  and  $A_b$  changes its sign.

Before closing this Section, we investigate the residual dependence of CP-even Higgs boson production in association with sbottoms and stops on the input values of  $M_0$  and  $M_{1/2}$ , when they are allowed to deviate from their common default of 150 GeV assumed so far. For illustrative purposes, we do so by adopting two discrete values of  $\tan\beta$ , 2 and 40, and choosing the combination  $A_0 = 0$  and negative  $\mu$ . Anyhow, though not shown, we have verified that a similar pattern to the one that we will outline below can be recognised also for the case of finite (positive and negative) values of  $A_0$  and positive Higgsino masses as well. For this exercise, we focus our attention only to the dominant production cross sections in either case, that is,  $\tilde{t}_1\tilde{t}_1^*h$ ,  $\tilde{t}_1\tilde{t}_2^*h$  and  $\tilde{b}_1\tilde{b}_1^*h$  for light (see Tab. 1) and  $\tilde{t}_1\tilde{t}_1^*H$  and  $\tilde{b}_1\tilde{b}_1^*H$  for heavy (see Tab. 2) Higgs bosons.

We obtain that most of the cross sections with the light Higgs particle involved decrease when either or both the parameters  $M_0$  and  $M_{1/2}$  increase. In this respect, however, it is well worth noticing that the total cross section for  $\tilde{t}_1\tilde{t}_2^*h$  production acquires a large statistic significance in the higher mass regime and maintains it even at the very upper end of it (some 5000 events/year can be produced at the LHC via this mode if  $\tan\beta = 2$ ,  $M_0 = 300$  GeV and  $M_{1/2} = 250$  GeV). In this area of the M-SUGRA parameter space,  $\tilde{t}_1\tilde{t}_2^*h$  events are much more numerous than  $\tilde{t}_1\tilde{t}_1^*h$  ones, the other way round with respect to the low mass combination  $M_0 = M_{1/2} = 130$  GeV, despite of the more massive final state. (However, this is only true at low  $\tan\beta$ .) In fact, for  $M_0 = 300$  GeV and  $M_{1/2} = 250$  GeV, the squark masses are  $m_{\tilde{t}_1} = 472$  GeV,  $m_{\tilde{t}_2} = 591$  GeV,  $m_{\tilde{b}_1} = 569$  GeV and  $m_{\tilde{b}_2} = 623$  GeV. The inversion of hierarchy between the two cross sections is induced by the onset of the  $\tilde{t}_2 \rightarrow \tilde{t}_1 h$  decay channel at large  $M_0$  and  $M_{1/2}$  values, as  $m_{\tilde{t}_2} \gtrsim m_{\tilde{t}_1} + m_h$ , whose resonance enhancement in the  $2 \rightarrow 2$  process  $gg \rightarrow \tilde{t}_2\tilde{t}_2^*$  overcomes both the inner phase space depletion and the strength of the Higgs-strahlung emission in  $gg \rightarrow \tilde{t}_1\tilde{t}_1^*$  events.

$M_0(\text{GeV})$	$M_{1/2}(\text{GeV})$	$\tan \beta$	$\sigma(gg \rightarrow \tilde{t}_1 \tilde{t}_1^* h)(\text{fb})$	$\sigma(gg \rightarrow \tilde{t}_1 \tilde{t}_2^* h)(\text{fb})$	$\sigma(gg \rightarrow \tilde{b}_1 \tilde{b}_1^* h)(\text{fb})$
130	130	2	70.2	38	$7.7 \times 10^{-2}$
200	150	2	32	150	$2.9 \times 10^{-2}$
200	200	2	11	100	$6.6 \times 10^{-3}$
300	250	2	2.9	48	$1.4 \times 10^{-3}$
130	130	40	84	8.2	8.2
200	150	40	37	7.4	4.9
200	200	40	13	3.4	1.3
300	250	40	3.5	1.8	0.51

Table 1: The variation of the most significant cross sections of processes  $gg \rightarrow \tilde{q}_\chi \tilde{q}_\chi^* h$  with  $M_0$ ,  $M_{1/2}$  and  $\tan \beta$ . The other M-SUGRA parameters are fixed as follows:  $A_0 = 0$  GeV and  $\text{sign}(\mu) = -$ .

As for the case  $\tilde{b}_1 \tilde{b}_1^* h$  (and similarly for  $\tilde{b}_2 \tilde{b}_2^* h$ , not shown in the table), there is no inversion of tendency here, in the interplay with the light stop channel, as production rates are strongly dominated by the fact that  $m_{\tilde{b}_2}, m_{\tilde{b}_1} \gg m_{\tilde{t}_1}$ . They both are very much suppressed. On similar grounds, one can argue about the smallness of  $\tilde{t}_2 \tilde{t}_2^* h$ . Finally, being  $m_{\tilde{b}_2} \lesssim m_{\tilde{b}_1} + m_h$  in most part of the  $(M_0, M_{1/2})$  plane that we have spanned, the  $\tilde{b}_2 \tilde{b}_1^* h$  final state never stands up either as quantitatively interesting.

The results for the mass dependence of the production rates for the heavy (CP-even) Higgs boson have a simpler pattern. The all of their production phenomenology is governed by the fact that over the  $(M_0, M_{1/2})$  regions considered here one never finds the kinematic configuration  $m_{t(\tilde{b})_2} \gtrsim m_{t(\tilde{b})_1} + m_H$ . That is, no production and decay channel can onset, and the hierarchy of cross sections already seen for  $M_0 = M_{1/2} = 150$  GeV replicates unaltered in most cases, mainly governed by the size of the rest masses in the final state. Here cross sections remain sizable only if neither  $M_0$  nor  $M_{1/2}$  exceed the value 150–200 GeV (for large  $\tan \beta$ , of course, see Fig. 5). Even in such cases, though, presumably no more than a handful of events can be selected in most decay channels.

#### 4.1.4 CP-odd Higgs boson production

As discussed to some length in Ref. [16], pseudoscalar Higgs boson production in association with sbottom and stop squarks of different mass (the only possible combination in absence of CP-violating phases in  $\mu$  and  $A_q$ , with  $q = t, b$ ), can boast a special attractiveness because of the absence of mixing terms in the relevant squark-squark-Higgs couplings. By making use of eq. (2) and recalling that if one reverts the chirality flow in the vertex  $\lambda_{A\tilde{q}_L\tilde{q}_R}$  the corresponding Feynman rule changes its sign [15], one finds that those vertices reduce to

$$\lambda_{A\tilde{t}_1\tilde{t}_2} = -\frac{g_W m_t}{2M_W} (\mu - A_t \cot \beta), \quad \lambda_{A\tilde{b}_1\tilde{b}_2} = -\frac{g_W m_b}{2M_W} (\mu - A_b \tan \beta). \quad (17)$$

$M_0(\text{GeV})$	$M_{1/2}(\text{GeV})$	$\tan \beta$	$\sigma(gg \rightarrow \tilde{t}_1 \tilde{t}_1^* H)(\text{fb})$	$\sigma(gg \rightarrow \tilde{b}_1 \tilde{b}_1^* H)(\text{fb})$
130	130	2	$8.0 \times 10^{-3}$	$2.1 \times 10^{-3}$
200	150	2	$1.4 \times 10^{-3}$	$4.2 \times 10^{-4}$
200	200	2	$1.1 \times 10^{-4}$	$7.5 \times 10^{-5}$
300	250	2	$1.3 \times 10^{-5}$	$8.2 \times 10^{-6}$
130	130	40	3.3	14
200	150	40	1.3	3.5
200	200	40	0.38	0.84
300	250	40	0.068	0.014

Table 2: The variation of the most significant cross sections (in pb) of processes  $gg \rightarrow \tilde{q}_\chi \tilde{q}_\chi^* H$  with  $M_0$ ,  $M_{1/2}$  and  $\tan \beta$ . The other M-SUGRA parameters are fixed as follows:  $A_0 = 0$  GeV and  $\text{sign}(\mu) = -$ .

These are precisely the couplings entering the two processes of the type (1) inducing the final states  $\tilde{q}_1 \tilde{q}_2^* A$ , where  $q = t, b$ .

From this point of view, it is then clear the potential of squark and pseudoscalar Higgs production in constraining the input values of all five M-SUGRA parameters. In other terms, to trace back (more technically, to fit) the shape of the cross sections (if not of some differential distributions) in terms of the  $\tan \beta$ ,  $A_q$  (with  $q = t, b$ ) and  $\mu$  parameters entering eq. (17) is presumably a much simpler job then doing the same by using the more involved expressions in eq. (2), unless one exploits some asymptotic regime in either  $\tan \beta$ ,  $A_q$  (with  $q = t, b$ ) and/or  $\mu$  in which the latter reduce to the former. It is under this perspective that we looked at the case of  $A$  production in our Ref. [16].

Rather than repeating the all discussion carried out there, we summarise here the salient findings of [16], referring the reader to that paper for specific details. The production cross sections can be found in Fig. 6. For  $\tan \beta$  below 20 or so, the rates for pseudoscalar Higgs boson production are presumably too poor to be of great experimental help. Furthermore, in the high  $\tan \beta$  regime, pseudoscalar Higgs boson production is in general less effective than other channels in constraining the sign of the Higgsino mass term: compare the overlapping for the solid and dot-dashed curves (for each  $A_0$ ) in the detectable regions of  $\tilde{t}_1 \tilde{t}_2^* A$  and  $\tilde{b}_1 \tilde{b}_2^* A$  production to the splitting occurring in, e.g.,  $\tilde{t}_1 \tilde{t}_1^* H$ . This, as far as it concerns the flaws.

As for the advantages, we would like to draw the attention of the reader to the fact that reactions (1) with CP-odd Higgs bosons in the final state are quite sensitive to  $\tan \beta$ . The simple form of the expressions for  $\lambda_{A\tilde{q}_1\tilde{q}_2}$  ( $q = t, b$ ) in eq. (17) allows one to straightforwardly interpret the variation of the pseudoscalar rates with this parameter, namely, the steep rise at high values of the latter. This can in fact be understood as follows. For large  $\tan \beta$ , the vertex couplings of eq. (17) can be rewritten in the approximate form

$$\lambda_{A\tilde{t}_1\tilde{t}_2} \simeq -\frac{g_W m_t}{2M_W} \mu, \quad \lambda_{A\tilde{b}_1\tilde{b}_2} \simeq \frac{g_W m_b}{2M_W} A_b \tan \beta, \quad (18)$$

that is, the coupling which is associated with the sbottom pair is proportional to  $\tan \beta$ , so



that, eventually, the total  $\tilde{b}_1\tilde{b}_2^*A$  cross section will grow with  $\tan^2\beta$  while the coupling related to the stop pair will assume constant values. In the latter, the enhancement of the  $\tilde{t}_1\tilde{t}_2^*A$  cross section with  $\tan\beta$  is rather a phase space effect since, as  $\tan\beta$  increases, the CP-odd Higgs boson mass decreases considerably (the squark masses changing much less instead), as we can see from Fig. 3. Of course, the same remains valid in the former case as well, so that our figure indicates a clear order in the size of the cross sections,  $\sigma(\tilde{b}_1\tilde{b}_2^*A) \gtrsim \sigma(\tilde{t}_1\tilde{t}_2^*A)$ , at large  $\tan\beta$ .

But, let us now turn our attention to another peculiar dependence of the production rates of  $\tilde{t}_1\tilde{t}_2^*A$  and  $\tilde{b}_1\tilde{b}_2^*A$ : the one on the common trilinear coupling  $A_0$ . Pretty much along the same lines as for the combinations  $\tilde{t}_1\tilde{t}_1^*h$ ,  $\tilde{t}_1\tilde{t}_2^*h$  and  $\tilde{b}_1\tilde{b}_1^*H$  one can make the case that the sensitivity to  $A_0$  of the  $A$  production cross sections offers the chance of constraining, possibly the sign, and hopefully the magnitude, of this fundamental M-SUGRA parameter. This is presumably the best attribute of  $\tilde{t}_1\tilde{t}_2^*A$  and  $\tilde{b}_1\tilde{b}_2^*A$ , under the assumption already made in few instances that the determination of  $\tan\beta$  could come first from studies in the pure Higgs sector. Putting down some numbers in this respect, one may invoke the following scenario, if  $\tan\beta$  is, say, larger than 32:

$$\sigma(\tilde{t}_1\tilde{t}_2^*A) \gtrsim 10 \text{ fb} \Rightarrow A_0 < -300 \quad (19)$$

$$\sigma(\tilde{b}_1\tilde{b}_2^*A) \gtrsim 2 \text{ fb} \Rightarrow A_0 < -300, \quad (20)$$

quite independently of  $\text{sign}(\mu)$ . Conversely, the non-observation of pseudoscalar Higgs events in those regimes would imply most likely a positive  $A_0$  value.

As for peculiar trends in Fig. 6, it is worth mentioning (though we have not shown it here, as the reader can refer to [16]) that the cross section for sbottom production vanishes too, at some (large) value of  $\tan\beta$ , as it did for the case of CP-even Higgs production. As the reader can appreciate in Fig. 2 of Ref. [16], contrary to the case of  $\tilde{b}_1\tilde{b}_2^*h$  and  $\tilde{b}_1\tilde{b}_2^*H$  final states, this however happens in  $\tilde{b}_1\tilde{b}_2^*A$  events only for positive and large values of  $A_0$  (and both  $\text{sign}(\mu) = \pm$ ). This is another consequence of the different nature of the couplings (2) to squarks of CP-even versus CP-odd neutral Higgs bosons. Though we have failed to find a point where this disappearance of  $\tilde{b}_1\tilde{b}_2^*A$  events for positive  $A_0$  values corresponds to the survival of a detectable cross section for negative  $A_0$ 's (at fixed  $\tan\beta$ ), such matter would presumably deserve further investigation in the future.

Before closing this Section, we study the dependence of pseudoscalar Higgs boson production in association with stop and sbottom squarks on the last two M-SUGRA independent parameters,  $M_0$  and  $M_{1/2}$ : see Tab. 3. The main effect of changing the latter is onto the masses of the final state scalars, through the phase space volume as well as via propagator effects in the scattering amplitudes. (In fact, no decay channel of the heavier stop or sbottom into the lighter one ever opens, at least for the values of  $M_0$  and  $M_{1/2}$  that we had looked at.) In other terms, to increase one or the other depletes both  $\sigma(\tilde{t}_1\tilde{t}_2^*A)$  and  $\sigma(\tilde{b}_1\tilde{b}_2^*A)$  quite strongly, simply because the values of all  $m_{\tilde{q}_X}$ 's,  $m_{\tilde{q}_{X'}}$ 's and  $m_\Phi$ 's get larger. For example, assuming  $\tan\beta = 40$ : at  $M_0 = M_{1/2} = 130$  GeV, one has  $m_{\tilde{t}_1} = 248$  GeV,  $m_{\tilde{t}_2} = 388$  GeV,  $m_{\tilde{b}_1} = 256$  GeV,  $m_{\tilde{b}_2} = 340$  GeV and  $m_A = 120$ ; whereas at  $M_0 = 300$  GeV and  $M_{1/2} = 250$  GeV, the figures are  $m_{\tilde{t}_1} = 461$  GeV,  $m_{\tilde{t}_2} = 611$  GeV,  $m_{\tilde{b}_1} = 510$  GeV,  $m_{\tilde{b}_2} = 591$  GeV and  $m_A = 292$  GeV. In practice, the table shows that only rather light  $M_0$  and  $M_{1/2}$  masses (say,

$M_0(\text{GeV})$	$M_{1/2}(\text{GeV})$	$\tan \beta$	$\sigma(gg \rightarrow \tilde{t}_1 \tilde{t}_2^* A)(\text{fb})$	$\sigma(gg \rightarrow \tilde{b}_1 \tilde{b}_2^* A)(\text{fb})$
130	130	2	$5.2 \times 10^{-2}$	$4.1 \times 10^{-4}$
200	150	2	$2.0 \times 10^{-2}$	$8.8 \times 10^{-5}$
200	200	2	$5.9 \times 10^{-3}$	$2.8 \times 10^{-5}$
300	250	2	$1.3 \times 10^{-3}$	$3.9 \times 10^{-6}$
130	130	40	79	13
200	150	40	1.4	2.4
200	200	40	0.31	0.6
300	250	40	0.048	0.098

Table 3: The variation of the most significant cross sections of processes  $gg \rightarrow \tilde{q}_\chi \tilde{q}_\chi^* A$  with  $M_0$ ,  $M_{1/2}$  and  $\tan \beta$ . The other M-SUGRA parameters are fixed as follows:  $A_0 = 0$  GeV and  $\text{sign}(\mu) = -$ .

below 200 and 150 GeV, respectively) would possibly allow for pseudoscalar production to be detectable at the LHC, and only at large  $\tan \beta$  [16].

#### 4.1.5 Charged Higgs bosons production

To have an additional source of charged Higgs bosons at the LHC, especially with masses larger than the top mass  $m_t$ , would be very helpful from an experimental point of view. In fact, it is well known the difficulty of detecting charged Higgs scalars in that mass regime, not only because of a dominant decay signature which suffers from very large QCD background (i.e.,  $H^\pm \rightarrow t\bar{b} \rightarrow b\bar{b}W^\pm \rightarrow b\bar{b}jj$ ), but also because the production mechanisms are not many and with not very large rates [13]. Unfortunately, as it turns out from Fig. 7, typical production cross sections of  $H^\pm$  scalars in association with sbottom and stop pairs rarely exceed 10 fb. These rates compare rather poorly with other mechanisms [13], for the same choice of  $m_{H^\pm}$ . Thus, there is little to gain in exploiting processes (1) as discovery channels of charged Higgs bosons.

Furthermore, their dependence on  $\tan \beta$ ,  $A_0$  and  $\text{sign}(\mu)$  replicates many of the tendencies already individuated in neutral Higgs channels, for which the production cross sections are much larger. Adding the fact that typical decay channels of the latter (e.g., in photon pairs) are much cleaner in the hadronic environment of the LHC than those of the former, one would quite rightly conclude that the potential of  $\tilde{t}_1 \tilde{b}_1^* H^-$ ,  $\tilde{t}_1 \tilde{b}_2^* H^-$ ,  $\tilde{b}_1 \tilde{t}_2^* H^+$  and  $\tilde{b}_2 \tilde{t}_2^* H^+$  final states in constraining the M-SUGRA parameter space is rather poor.

Nonetheless, it is worth recognising some of the typical trends of the production cross sections, for the sake of future reference. Let alone the last two combinations, for which the final state masses are too heavy to be produced at detectable rate, we have a quick look at the first two cases, which can indeed have cross sections significantly above 1 fb, at least in the large  $\tan \beta$  region. This enhancement has a twofold explanation. Firstly, phase space effects, as for large  $\tan \beta$  all scalar masses (except  $m_{\tilde{t}_1}$  and  $m_h$ ) get smaller: see Figs. 2–3.

$M_0(\text{GeV})$	$M_{1/2}(\text{GeV})$	$\tan\beta$	$\sigma(gg \rightarrow \tilde{t}_1 \tilde{b}_1^* H^-)(\text{fb})$	$\sigma(gg \rightarrow \tilde{t}_1 \tilde{b}_2^* H^-)(\text{fb})$
130	130	2	$4.3 \times 10^{-4}$	$1.4 \times 10^{-3}$
200	150	2	$2.2 \times 10^{-5}$	$3.0 \times 10^{-4}$
200	200	2	$3.1 \times 10^{-5}$	$9.8 \times 10^{-5}$
300	250	2	$1.6 \times 10^{-6}$	$1.4 \times 10^{-5}$
130	130	40	2.2	4.8
200	150	40	1.5	4.5
200	200	40	1.7	0.31
300	250	40	0.064	0.023

Table 4: The variation of the most significant cross sections of processes  $gg \rightarrow \tilde{q}_\chi \tilde{q}_\chi^* H^\pm$  with  $M_0$ ,  $M_{1/2}$  and  $\tan\beta$ . The other M-SUGRA parameters are fixed as follows:  $A_0 = 0$  GeV and  $\text{sign}(\mu) = -$ .

Secondly, terms in their couplings proportional to  $m_b A_b \tan\beta$  are dominant for most of the possible  $A_0$  and  $\text{sign}(\mu)$  combinations. Finally, notice also in the case of the  $\tilde{t}_1 \tilde{b}_1^* H^\pm$  final state the vanishing of the cross section, this time at somewhat lower values of  $\tan\beta$  than in the case of the neutral Higgs bosons.

As for the  $M_0$  and  $M_{1/2}$  dependence, this is again realised through the phase space and the propagators, as there is no significant enhancement from resonant decays. In practice, only if  $\tan\beta$  is extremely large and both the universal scalar and gaugino masses are below 200 GeV, the two cross sections for  $\tilde{t}_1 \tilde{b}_1^* H^-$  and  $\tilde{t}_1 \tilde{b}_2^* H^-$  remain detectable (indeed, those containing the lightest stop squark): see Tab. 4.

#### 4.1.6 Decay signatures

So far we have only discussed production cross sections for processes of the form (1) and made no considerations about possible decay channels and relative branching fractions of either squarks or Higgs bosons. Another related aspect is the typical kinematics of the signals, as it appears in the detectors, and the size of the possible backgrounds. Furthermore, the reader should appreciate how all channels entering processes (1) are intertwined, in the sense that any of these can act as a background to all others.

It is the aim of this Section that of indicating some possible decay signatures of the most relevant squark-squark-Higgs processes, in which they show both large rates and their kinematics is such that they can hopefully be disentangled at the LHC. In doing so, we distinguish between a small (see 4.1.6.1) and large (see 4.1.6.2)  $\tan\beta$  regime, as we have shown that such a parameter is crucial in determining the actual size of the production rates. As representative choice of the universal masses we adopt the combination with lowest values among those discussed in the previous Subsections, i.e.,  $M_0 = M_{1/2} = 130$  GeV, further setting  $A_0=0$  and  $\text{sign}(\mu)$  negative.

#### 4.1.6.1 Small $\tan\beta$ regime

For small  $\tan\beta$ 's the only relevant processes are  $\tilde{t}_1\tilde{t}_1^*h$  and  $\tilde{t}_1\tilde{t}_2^*h$  production. A possible decay signature for the first case is the one contemplated in Refs. [17, 18]. That is,  $\tilde{t}_1 \rightarrow \chi_1^+ b \rightarrow W^+ b$  plus missing energy for the light stop and  $h \rightarrow \gamma\gamma$  for the light Higgs boson, with the  $W^+$  decaying leptonically and/or hadronically. The final topology would be the same as in  $t\bar{t}h$ , with the only difference that for stop squark events there is a large amount of missing energy.

Since another option to tag the lightest MSSM Higgs boson at the LHC is to use the more messy but dominant decay channel into  $b\bar{b}$  pairs (as opposed to exploiting the cleaner but suppressed  $\gamma\gamma$  mode) [39, 40], another possible decay sequence could be the following:

$$\begin{array}{ccc}
\tilde{t}_1 & \tilde{t}_1^* & h \\
\downarrow & \downarrow & \downarrow \\
\chi_1^+ + b & \chi_1^- + \bar{b} & b + \bar{b} \\
\downarrow & \downarrow & \\
q + \bar{q}' + \chi_1^0 & \ell^- + \nu + \chi_1^0 & 
\end{array}$$

in which  $q\bar{q}' = u\bar{d}, c\bar{s}$  and  $\ell = e, \mu$ . Considering also the charge conjugated  $\chi_1^+ \chi_1^-$  decays, the final signature would then be ‘2 jets +  $4b + \ell^\pm + E_{\text{miss}}$ ’, where the missing energy/momentum is not only due to the two  $\chi_1^0$ 's but also to the neutrinos.

The total branching ratio (BR) of such a decay sequence is, for  $\tan\beta = 3$  and according to Tab. 5, approximately 2.5%. The production cross section at the same  $\tan\beta$  value is about 72 fb, so that about 176 events per year would survive. One may further assume a reduction factor of about 0.25 because of the overall efficiency  $\varepsilon_b^4$  to tag four  $b$ -quarks (assuming  $\varepsilon_b \approx 0.7$ ). This ultimately yields something more than 44 events per year. In addition, one should expect most of the signal events to lie in the detector acceptance region, since leptons and jets originate from decays of heavy objects.

The same signature could well be exploited in the case of the  $\tilde{t}_1\tilde{t}_2^*h$  final state. Here, the production cross section is smaller than for  $\tilde{t}_1\tilde{t}_1^*h$  production, about 40 fb, so is the  $\tilde{t}_2 \rightarrow \chi_1^+ b$  decay rate as compared to the  $\tilde{t}_1 \rightarrow \chi_1^+ b$  one (see Tab. 5). However, the final number of events per year is still quite large: about 14 after having already multiplied by  $\varepsilon_b^4$ .

As for the kinematics of these two signatures, we may remark that they have peculiar features that should help in their selection: a not too large hadronic multiplicity, six jets in total, each rather energetic (in fact, note that  $m_{\chi_1^\pm} - m_{\chi_1^0} \approx 58$  GeV and  $m_{\tilde{t}_2} \approx 378$  GeV  $\gg m_{\tilde{t}_1} \approx 273$  GeV  $\gg m_{\chi_1^\pm} \approx 114$  GeV), so that their reconstruction from the detected tracks should be reasonably accurate; high transverse momentum and isolated leptons to be used as trigger; large  $E_{\text{miss}}$  to reduce non-SUSY processes; four tagged  $b$ -jets that can be exploited to suppress the ‘ $W^\pm + \text{light jet}$ ’ background from QCD, and one  $b\bar{b}$  pair resonating at the  $h$  mass,  $m_h \approx 90$  GeV. Moreover, the ‘irreducible’ background from  $\tilde{t}_1\tilde{t}_1^*Z$  events has been shown in Ref. [19] to be under control, even when  $m_h \approx M_Z$ , as it is the case here.

Particle	BR	Decay
$\tilde{t}_1$	$\xrightarrow{76\%}$	$\chi_1^+ b$
	$\xrightarrow{19\%}$	$\chi_1^0 t$
$\tilde{t}_2$	$\xrightarrow{57\%}$	$\chi_1^+ b$
	$\xrightarrow{24\%}$	$\chi_2^+ b$
	$\xrightarrow{11\%}$	$\chi_2^0 t$
$h$	$\xrightarrow{90\%}$	$b\bar{b}$
	$\xrightarrow{5\%}$	$\tau^+ \tau^-$
	$\xrightarrow{0.0003\%}$	$\gamma\gamma$

Particle	BR	Decay
$t$	$\xrightarrow{33\%}$	$u\bar{d}b$
	$\xrightarrow{33\%}$	$c\bar{s}b$
	$\xrightarrow{11\%}$	$e^+ \nu b$
	$\xrightarrow{11\%}$	$\mu^+ \nu b$
	$\xrightarrow{11\%}$	$\tau^+ \nu b$
$\chi_1^+$	$\xrightarrow{30\%}$	$\chi_1^0 u d^\dagger$
	$\xrightarrow{30\%}$	$\chi_1^0 c \bar{s}^\dagger$
	$\xrightarrow{14\%}$	$\chi_1^0 \tau^+ \nu^\dagger$
	$\xrightarrow{14\%}$	$\chi_1^0 e^+ \nu^\dagger$
	$\xrightarrow{14\%}$	$\chi_1^0 \mu^+ \nu^\dagger$
$\chi_2^0$	$\xrightarrow{28\%}$	$\chi_1^0 \nu \bar{\nu}$
	$\xrightarrow{14\%}$	$\chi_1^0 e^- e^+$
	$\xrightarrow{14\%}$	$\chi_1^0 \mu^- \mu^+$
	$\xrightarrow{14\%}$	$\chi_1^0 \tau^- \tau^+$

Table 5: Dominant decay channels and BRs of the final state (s)particles in  $gg \rightarrow \tilde{q}_\chi \tilde{q}_{\chi'}^* h$ ,  $q = t$  and  $\chi, \chi' = 1, 2$ , for  $M_0 = M_{1/2} = 130$  GeV,  $A_0 = 0$ ,  $\tan \beta = 3$  and  $\text{sign}(\mu) < 0$  [10].

<sup>†</sup> Via off-shell  $W^+$ .

Particle	BR	Decay
$\tilde{t}_1$	$\xrightarrow{94\%}$	$\chi_1^+ b$
$\tilde{t}_2$	$\xrightarrow{40\%}$	$\chi_2^+ b$
	$\xrightarrow{26\%}$	$\chi_1^+ b$
	$\xrightarrow{16\%}$	$\tilde{b}_1 W^+$
	$\xrightarrow{7\%}$	$\tilde{t}_1 Z$
$\tilde{b}_1$	$\xrightarrow{61\%}$	$\chi_2^0 b$
	$\xrightarrow{32\%}$	$\chi_1^0 b$
$\tilde{b}_2$	$\xrightarrow{42\%}$	$\chi_3^0 b$
	$\xrightarrow{31\%}$	$\chi_4^0 b$
	$\xrightarrow{18\%}$	$\chi_2^0 b$
$h$	$\xrightarrow{94\%}$	$b\bar{b}$
	$\xrightarrow{6\%}$	$\tau^+ \tau^-$
$H$	$\xrightarrow{94\%}$	$b\bar{b}$
	$\xrightarrow{6\%}$	$\tau^+ \tau^-$
$A$	$\xrightarrow{94\%}$	$b\bar{b}$
	$\xrightarrow{6\%}$	$\tau^+ \tau^-$
$H^\pm$	$\xrightarrow{91\%}$	$\tau^\pm \nu$
	$\xrightarrow{5\%}$	$\chi_1^0 \chi_1^\pm$

Particle	BR	Decay
$\chi_1^+$	$\xrightarrow{100\%}$	$\tilde{\tau}_1^+ \nu$
$\chi_2^+$	$\xrightarrow{24\%}$	$\chi_2^0 W^+$
	$\xrightarrow{15\%}$	$\chi_1^+ Z$
	$\xrightarrow{11\%}$	$\chi_1^+ A$
	$\xrightarrow{10\%}$	$\tau^+ \tilde{\nu}$
$\chi_2^0$	$\xrightarrow{100\%}$	$\tilde{\tau}_1^\pm \tau^\mp$
$\chi_3^0$	$\xrightarrow{24\%}$	$\chi_1^+ W^-$
	$\xrightarrow{24\%}$	$\chi_1^- W^+$
	$\xrightarrow{9\%}$	$\chi_1^0 Z$
$\chi_4^0$	$\xrightarrow{23\%}$	$\chi_1^+ W^-$
	$\xrightarrow{23\%}$	$\chi_1^- W^+$
	$\xrightarrow{6\%}$	$\chi_1^0 h$
	$\xrightarrow{6\%}$	$\chi_1^0 Z$
$\tilde{\tau}_1^+$	$\xrightarrow{100\%}$	$\chi_1^0 \tau^+$

Table 6: Dominant decay channels and BRs of the final state (s)particles in  $gg \rightarrow \tilde{q}_\chi \tilde{q}_{\chi'}^* X$ ,  $X = h, H, A, H^\pm$ ,  $q = t, b$  and  $\chi, \chi' = 1, 2$ , for  $M_0 = M_{1/2} = 130$  GeV,  $A_0 = 0$ ,  $\tan \beta = 40$  and  $\text{sign}(\mu) < 0$  [10].

#### 4.1.6.2 Large $\tan \beta$ regime

In the large  $\tan \beta$  regime there is a variety of cross sections which can be significant:  $\tilde{t}_1 \tilde{t}_1^* X$ ,  $\tilde{t}_1 \tilde{t}_2^* X$ ,  $\tilde{b}_1 \tilde{b}_1^* X$ ,  $\tilde{b}_2 \tilde{b}_2^* X$ ,  $\tilde{t}_1 \tilde{t}_2^* A$ ,  $\tilde{b}_1 \tilde{b}_2^* A$ ,  $\tilde{t}_1 \tilde{b}_1^* H^+$  and  $\tilde{t}_1 \tilde{b}_2^* H^+$ , where  $X = h, H$ . For reasons of space, however, we only focus our attention to one signature for the Higgs states not yet considered, the one arising from the dominant production channel in all cases, with the only exception of the charged Higgs bosons. In fact, we will neglect analysing here their decay patterns, as we have already mentioned the poor effectiveness of the charged Higgs production modes both as discovery channels and probes of the underlying M-SUGRA model.

In the case of heavy scalar Higgs bosons, we consider the final state  $\tilde{b}_1 \tilde{b}_1^* H$ . This yields a cross section of 14 fb for  $\tan \beta = 40$ . A possible decay chain is the one below.

$$\begin{array}{ccc} \tilde{b}_1 & \tilde{b}_1^* & H \\ \downarrow & \downarrow & \downarrow \\ \chi_1^0 + b & \chi_1^0 + \bar{b} & b + \bar{b} \end{array}$$

That is, a rather simple final state made up by four  $b$ -quarks and missing energy. The BR of this sequence is about 9% (see Tab. 6). Therefore, at high luminosity, one obtains 129 events per year, before heavy flavour identification.

The main background is certainly ordinary QCD production of four jets. However, the requirement of tagging four  $b$ -jets would reduce the latter considerably. Furthermore, if the mass of the heavy scalar Higgs boson is known, then one could impose that two  $b$ -quarks reproduce  $m_H \approx 121$  GeV within a few GeV (say, 5) in invariant mass. Finally, given the enormous mass difference  $m_{\tilde{b}_1} - m_b \approx 250$  GeV, compared to the rest mass of the LSP,  $m_{\tilde{\chi}_1^0} \approx 51$  GeV, one should expect, on the one hand, a large amount of missing energy, and, on the other hand, all four  $b$ -jets to be quite hard, both aspects further helping to reduce the QCD noise. In the end, some 32 events could well be detected annually, having already accounted for the overall  $b$ -tagging efficiency  $\varepsilon_b^4 = 0.25$ .

For the case of the pseudoscalar Higgs particle, we choose the final state  $\tilde{t}_1 \tilde{t}_2^* A$ , which has a cross section of about 79 fb at  $\tan \beta = 40$ . A possible signature could be<sup>9</sup>:

$$\begin{array}{ccc} \tilde{t}_1 & \tilde{t}_2^* & A \\ \downarrow & \downarrow & \downarrow \\ \chi_1^+ + b & \chi_1^- + \bar{b} & b + \bar{b} \\ \downarrow & \downarrow & \\ \tilde{\tau}_1 + \nu & \tilde{\tau}_1^* + \bar{\nu} & \\ \downarrow & \downarrow & \\ \tau^+ + \chi_1^0 & \tau^- + \chi_1^0 & \end{array}$$

Here, the final state is made up by four  $b$ -quarks and two  $\tau$ 's, plus missing energy as usual. The decay fraction is 23% (again, see Tab. 6). That is, 1814 events per year before tagging  $b$ 's and  $\tau$ 's.

---

<sup>9</sup>Additional examples can be found in Ref. [16].

The most dangerous backgrounds are probably  $Z + 4$  jet production and  $t\bar{t}b\bar{b}$  events. The first can be rejected by asking, e.g.,  $M_{\tau^+\tau^-} \neq M_Z$ , if  $\tau$ 's are reconstructed. In addition, both background processes have (at least) two  $b$ -quarks quite soft. As for the signal, given that the lightest chargino mass is much smaller than the stop ones (in fact,  $m_{\tilde{\chi}_1^\pm} \approx 93$  GeV whereas  $m_{\tilde{t}_1} \approx 248$  GeV and  $m_{\tilde{t}_2} \approx 388$  GeV), all  $b$ 's are naturally energetic and two of them also peak at  $m_A \approx 120$  GeV. Thus, to require all  $M_{bb}$  invariant masses sufficiently large with one close to the  $A$  mass should help in enhancing considerably the signal-to-background rates. Requiring large missing energy would help further, especially against  $t\bar{t}b\bar{b}$  events. More difficult is to discern differences in the  $\tau$  behaviours (though, notice that  $m_{\tilde{\tau}_1} \approx 76$  GeV  $\gg m_\tau$ ). For  $\varepsilon_b^4 = 0.25$ , and assuming leptonic decays of both  $\tau^+$  and  $\tau^-$  into electrons and/or muons, one finally gets something of the order of 110 signal events per year.

## 4.2 Heavy mass spectrum

An attempt to summarise our findings is made in Fig. 8, where the most relevant cross sections (see upper frame) for the light mass regime (see lower frame) are plotted for a choice of  $M_0$ ,  $M_{1/2}$ ,  $A_0$ ,  $\tan\beta$  and  $\text{sign}(\mu)$  which reflects their hierarchal order seen over most of the M-SUGRA parameter space discussed so far.

However, to assume that only light squark and Higgs masses can induce sizable cross sections in events of the type (1) would be wrong. This is a sufficient condition for many channels, but not a necessary one. For example, even for very large universal masses, one could find a value of the soft trilinear coupling small enough to overcome the loss of signal due to propagator and phase space effects. In fact, as repeatedly shown in the previous Section, most of the cross sections considered here grow quickly as  $A_0$  becomes negative. Fig. 9 makes eloquently this point (top insert), for the choice  $A_0 = -900$  GeV, well consistent with the bounds imposed by the charge and colour breaking minima. There, we have adopted a very large value for  $M_0$ , i.e., 500 GeV, and varied  $M_{1/2}$  between 100 and 500 GeV. The choice of a large  $\tan\beta$  value, i.e., 35, is necessary to obtain detectable rates, except in those cases involving  $\tilde{t}_1$  and  $h$  in the same event. In contrast, that of a negative  $\text{sign}(\mu)$  never is. The squark and Higgs masses produced by the above combinations of M-SUGRA parameters can be found in the bottom frame of Fig. 9.

There are only a few production channels which survive the strong phase space suppression arising in the heavy mass regime and yield cross sections above 1 fb. Among these, other than those already encountered  $\tilde{t}_1\tilde{t}_1^*h$ ,  $\tilde{t}_1\tilde{t}_2^*h$ ,  $\tilde{b}_1\tilde{b}_1^*h$ , one notices the appearance of channels which had negligible rates in the low mass regime, notably  $\tilde{b}_1\tilde{b}_2^*h$  (compare to Fig. 4). In this specific instance, the effect is due to the enhancement induced by the onset of the  $\tilde{b}_2 \rightarrow \tilde{b}_1h$  decay mode in  $gg \rightarrow \tilde{b}_2\tilde{b}_2^*$  events. Even the other two combinations  $\tilde{t}_1\tilde{t}_1^*H$  and  $\tilde{t}_1\tilde{b}_2^*H^-$ , which had a rather low profile in the light mass regime, now compete more closely with the dominant modes. Finally, notice that pseudoscalar Higgs boson production is no longer significant in this mass regime, in line with the results presented in Ref. [16].

In practise, if  $M_0 = 500$  GeV, events involving light CP-even Higgs bosons could be detected up to  $M_{1/2} = 400$  GeV or so, in either mode  $\tilde{t}_1\tilde{t}_1^*h$  or  $\tilde{t}_1\tilde{t}_2^*h$ . Final states of the type  $\tilde{b}_1\tilde{b}_2^*h$  have surprisingly large rates if  $M_{1/2}$  is below 220 GeV. The maximum reach in  $M_{1/2}$



via  $\tilde{b}_1\tilde{b}_1^*h$ ,  $\tilde{t}_1\tilde{b}_2^*H^-$  and  $\tilde{t}_1\tilde{t}_1^*H$  is instead 220, 180 and 140 GeV, respectively.

This is just one example where a new phenomenology of squark-squark-Higgs events arises for rather heavy  $M_0$  and  $M_{1/2}$  masses. We have found several such combinations, and linked them to the fact that  $A_0$  ought to be significantly large and negative,  $\tan\beta$  close to  $m_t/m_b$ , but with small dependence on  $\text{sign}(\mu)$ .

## 5 Conclusions

In summary, we have studied neutral and charged Higgs boson production in association with all possible combinations of stop and sbottom squarks at the LHC, in the context of the SUGRA inspired MSSM. Our interest in such reactions was driven not only by the fact that they can act as new sources of Higgs particles but also because they carry a strong dependence on the five inputs of the SUSY model, so that they can possibly be used to constrain the latter. In a sense, this note (along with Ref. [16]) completes previous analyses on the subject [17, 18, 19], where the emphasis was mainly put on the usefulness of the above kind of reactions as Higgs production modes and the attention consequently restricted to the case of light squark and Higgs masses.

We have found that the cross sections of many of these processes should be detectable at high collider luminosity for not too small values of  $\tan\beta$ . Indeed, their production rates are strongly sensitive to the ratio of the VEVs of the Higgs fields, this possibly allowing one to put potent constraints on such a crucial parameter of the MSSM Higgs sector. Furthermore, also the trilinear coupling  $A_0$  intervenes in these events, in such a way that visible rates would mainly be possible if this other fundamental M-SUGRA input is negative. (Indeed, to know the actual value of  $\tan\beta$  from other sources would further help to assess the magnitude of  $A_0$ .) As for the sign of the Higgsino mass term,  $\text{sign}(\mu)$ , it affects the phenomenology of such events in one or two channels only, so that it can easily evade the imposition of experimental bounds. Finally, concerning the remaining two parameters (apart from mixing effects) of the M-SUGRA scenario, one must say that  $M_0$  need not be small (it could be as large as 500 GeV) and that  $M_{1/2}$  is enough to be below 220 GeV in order to guarantee sizable cross sections in many cases.

In a few representative examples, we have further investigated the decay phenomenology of these reactions, by discussing some possible signatures, their rates (of the order of tens to hundreds of events per year at high luminosity) and peculiar kinematics, as opposed to the yield of ordinary, non-SUSY backgrounds.

In conclusion, we believe these processes to be potentially very helpful in putting drastic limits on several M-SUGRA parameters and we thus recommend that their phenomenology is further investigated in the context of dedicated experimental simulations, which were clearly beyond the scope of this note. In this spirit, we have derived compact analytical formulae of the relevant production MEs, that can easily be incorporated in existing MC programs.

## Acknowledgements

S.M. acknowledges the financial support from the UK PPARC and useful conversations with Michael Krämer. A.D is supported from the Marie Curie Research Training Grant ERB-FMBI-CT98-3438 and thanks Mike Seymour for useful discussions. We both thank Herbi Dreiner for precious comments and The Old School in Oxford for kind hospitality.

## References

- [1] M. Carena, R.L. Culbertson, S. Eno, H.J. Frisch and S. Mrenna, preprint ANL-HEP-PR-97-98, December 1997, [hep-ex/9712022](#) and references therein.
- [2] F.E. Paige, preprint BNL-HET-98-1, C97-06-01, December 1997, [hep-ph/9801254](#) and references therein, to appear in Theoretical Advanced Study Institute in Elementary Particle Physics (TASI 97): ‘Supersymmetry, Supergravity and Supercolliders’, Boulder, CO, USA, 1-7 June 1997.
- [3] G.L. Kane and J.P. Leveille, Phys. Lett. **B112** (1982) 227;  
P.R. Harrison and C.H. Llewellyn-Smith, Nucl. Phys. **B213** (1983) 223; Erratum, *ibidem* **223** (1983) 542;  
E. Reya and D.P. Roy, Phys. Rev. **D32** (1985) 645;  
S. Dawson, E. Eichten and C. Quigg, Phys. Rev. **D31** (1985) 1581;  
H. Baer and X. Tata, Phys. Lett. **B160** (1985) 159;  
W. Beenakker, R. Höpker, M. Spira and P.M. Zerwas, Phys. Rev. Lett. **74** (1995) 2905;  
Nucl. Phys. **B492** (1997) 51;  
W. Beenakker, M. Krämer, T. Plehn, M. Spira and P.M. Zerwas, Nucl. Phys. **B515** (1998) 3.
- [4] J.F. Gunion, H.E. Haber, G.L. Kane and S. Dawson, “The Higgs Hunter Guide” (Addison-Wesley, Reading MA, 1990) and references therein.
- [5] I. Hinchliffe, F.E. Paige, M.D. Shapiro, J. Söderqvist and W. Yao, Phys. Rev. **D55** (1997) 5520.
- [6] See, e.g.:  
P. Nath, invited review talk given at ‘SUSY 97’, University of Pennsylvania, Philadelphia, 17-21 May 1997, preprint NUB-TH-3167/97, [hep-ph/9708221](#), Nucl. Phys. Proc. Suppl. **62** (1998) 119 and references therein.
- [7] H.P. Nilles, Phys. Rep. **111** (1984) 1;  
H.E. Haber and G.L. Kane, Phys. Rep. **117** (1985) 75;  
A.B. Lahanas and D.V. Nanopoulos, Phys. Rep. **145** (1987) 1;  
R. Barbieri, Riv. Nuov. Cim. Vol. **11** No. 4 (1988) 1.
- [8] L. E. Ibañez and G. G. Ross, Phys. Lett. **110** (1982) 215;  
K. Inoue, A. Kakuto, H. Komatsu and S. Takeshita, Progr. Theor. Phys. **68** (1982) 927;

- ibidem **71** (1984) 96;  
 J. Ellis, D. V. Nanopoulos and K. Tamvakis, Phys. Lett. **B121** (1983) 123;  
 L. E. Ibañez, Nucl. Phys. **B218** (1983) 514;  
 L. Alvarez-Gaumé, J. Polchinski and M. Wise, Nucl. Phys. **B221** (1983) 495;  
 J. Ellis, J.S. Hagelin, D.V. Nanopoulos and K. Tamvakis, Phys. Lett. **B125** (1983) 275;  
 L. Alvarez-Gaumé, M. Claudson and M. Wise, Nucl. Phys. **B207** (1982) 96;  
 C. Kounnas, A. B. Lahanas, D. V. Nanopoulos and M. Quiros, Phys. Lett. **B132** (1983) 95;  
 L. E. Ibañez and C. E. Lopez, Phys. Lett. **B126** (1983) 54; Nucl. Phys. **B233** (1984) 511.
- [9] See, e.g.:  
 G.G. Ross, “Grand Unified Theories” (Benjamin-Cummings, 1984) and references therein.
- [10] F.E. Paige, S.D. Protopopescu, H. Baer and X. Tata, preprint BNL-HET-98/18, FSU-HEP-980417, UH-511-899-98, April 1998, [hep-ph/9804321](#); preprint BNL-HET-98/39, FSU-HEP-981016, UH-511-917-98, October 1998, [hep-ph/9810440](#).
- [11] T. Sjöstrand, Comp. Phys. Commun. **82** (1994) 74;  
 T. Sjöstrand, Comp. Phys. Commun. **39** (1986) 347;  
 M. Bengtsson and T. Sjöstrand, Comp. Phys. Commun. **43** (1987) 367;  
 S. Mrenna, Comp. Phys. Commun. **101** (1997) 232;  
 the latest program version and documentation is found at:  
<http://www.thep.lu.se/tf2/staff/torbjorn/Pythia.html>.
- [12] G. Marchesini and B.R. Webber, Nucl. Phys. **B310** (1988) 461;  
 G. Marchesini, B.R. Webber, G. Abbiendi, I.G. Knowles, M.H. Seymour and L. Stanco, Comp. Phys. Commun. **67** (1992) 465;  
 G. Marchesini, B.R. Webber, I.G. Knowles, M.H. Seymour, G. Corcella, S. Moretti, K. Odagiri and P. Richardson, in preparation.
- [13] J.F. Gunion, H.E. Haber, F.E. Paige, W.-K. Tung and S.S.D. Willenbrock, Nucl. Phys. **B294** (1987) 621;  
 J.L. Diaz-Cruz and O.A. Sampayo, Phys. Rev. **D50** (1994) 6820;  
 S. Moretti and K. Odagiri, Phys. Rev. **D55** (1997) 5627;  
 A.A. Barrientos Bendezú and B.A. Kniehl, Phys. Rev. **D59** (1999) 015009;  
 S. Moretti and K. Odagiri, Phys. Rev. **D59** (1999) 055008;  
 D.J. Miller, S. Moretti, D.P. Roy and W.J. Stirling, preprint RAL-TR-1999-029, April 1999.
- [14] H. Georgi, S.L. Glashow, M.E. Machacek and D.V. Nanopoulos, Phys. Rev. Lett. **40** (1978) 692;  
 M. Spira, A. Djouadi, D. Graudenz and P.M. Zerwas, Nucl. Phys. **B453** (1995) 17.
- [15] J.F. Gunion, H.E. Haber, G.L. Kane and S. Dawson, in Ref. [4];  
 J. Rosiek, Phys. Rev. **D41** (1990) 3464; Erratum, [hep-ph/9511250](#).

- [16] A. Dedes and S. Moretti, preprint RAL-TR-1998-081, December 1998, *to appear in Phys. Rev. D*, [hep-ph/9812328](#).
- [17] A. Djouadi, J.-L. Kneur and G. Moultaka, *Phys. Rev. Lett.* **80** (1998) 1830.
- [18] A. Djouadi, J.-L. Kneur and G. Moultaka, preprint PM/98-40, March 1999, [hep-ph/9903218](#).
- [19] G. Bélanger, F. Boudjema and K. K. Sridhar, preprint LAPTH-730/99, TIFR/TH/99-17, April 1999, [hep-ph/9904348](#).
- [20] G. Bélanger, talk given at the ‘2th ECFA/DESY Study on Physics and Detectors for a Linear Electron-Positron Collider’, LNF, Frascati, Italy, 8-10 November 1998;  
J.-L. Kneur, talk given at the ‘2th ECFA/DESY Study on Physics and Detectors for a Linear Electron-Positron Collider’, LNF, Frascati, Italy, 8-10 November 1998;  
G. Bélanger, F. Boudjema, T. Kon, V. Lafage, [hep-ph/9811334](#).
- [21] H.E. Haber, talk given at the ‘Beyond the Standard Model Conference’, Lake Tahoe, CA, USA, 13-18 December 1994; and at the ‘Ringsberg Workshop on Perspectives for Electroweak Interactions in  $e^+e^-$  Collisions’, Ringsberg, Germany, 5-8 February 1995, preprint CERN-TH-95-109, SCIPP-95-15, April 1995, [hep-ph/9505240](#).
- [22] G.P. Lepage, *Jour. Comp. Phys.* **27** (1978) 192.
- [23] H.L. Lai, J. Huston, S. Kuhlmann, F. Olness, J.F. Owens, D. Soper, W.K. Tung and H. Weerts, *Phys. Rev.* **D55** (1997) 1280.
- [24] A.D. Martin, R.G. Roberts, W.J. Stirling and R.S. Thorne, *Phys. Lett.* **B443** (1998) 301.
- [25] For some reviews, see, e.g.:  
A. Masiero and L. Silvestrini, lecture given at the ‘International School on Subnuclear Physics, 35th Course’, “Highlights: 50 Years Later”, Erice, Italy, 26 August-4 September 1997 and at the ‘International School of Physics Enrico Fermi, Course CXXVII’, “Heavy flavour physics: a probe of Nature’s grand design”, Varenna, Italy, 8-18 July 1997, preprint TUM-HEP-303/97, December 1997, [hep-ph/9711401](#);  
Y. Grossman, Y. Nir and R. Rattazzi, preprint SLAC-PUB-7379, WIS-96/49/Dec-PH, CERN-TH/96-368, to appear in the Review Volume “Heavy Flavours II”, eds. A.J. Buras and M. Lindner, Advanced Series on Directions in High Energy Physics, World Scientific Publishing Co., Singapore, April 1997, [hep-ph/9701231](#).
- [26] A. Dedes, A.B. Lahanas and K. Tamvakis, *Phys. Rev.* **D53** (1996) 3793.
- [27] S. Navas-Concha, talk given at ‘SUSY 98’, Keble College, Oxford, UK, 11-17 July 1998.
- [28] The ALEPH Collaboration, talk given at the ‘XXIXth International Conference on High Energy Physics’, Vancouver, Canada, 23-29 July 1998, preprint ALEPH 98-075.

- [29] C. Kounnas, A. Lahanas, D. Nanopoulos and M. Quiros, Nucl. Phys. **B236** (1984) 438;  
J. F. Gunion, H. E. Haber and M. Sher, Nucl. Phys. **B306** (1988) 1;  
J. A. Casas, A. Lleyda, C. Muñoz, Nucl. Phys. **B471** (1996) 3.
- [30] J. Erler, talk presented at the DPF'99 meeting, Los Angeles, CA, 5-9 January 1999,  
preprint [hep-ph/9903449](#);  
G. Altarelli, preprint CERN-TH/98-348, November 1998, [hep-ph/9811456](#).
- [31] A. Dedes, A. B. Lahanas and K. Tamvakis, Phys. Rev. **D59** (1999) 5019.
- [32] P. Chankowski, S. Pokorski and J. Rosiek, Nucl. Phys. **B423** (1994) 437;  
V. Barger, M.S. Berger and P. Ohmann, Phys. Rev. **D49** (1994) 4908;  
M. Drees and S.P. Martin, contribution to the DPF long range study, working group on  
'Electroweak Symmetry Breaking and Beyond the SM Physics', preprint MAD-PH-879,  
UM-TH-95-02, April 1995, [hep-ph/9504324](#);  
D. Pierce, J. Bagger, K. Matchev and R.J. Zhang, Nucl. Phys. **B491** (1997) 3.
- [33] DØ Collaboration, preprint Fermilab-Pub-99-046-E, March 1999, [hep-ex/9903041](#).
- [34] ALEPH Collaboration, Phys. Lett. **B434** (1998) 189;  
OPAL Collaboration, Eur. Phys. J. **C6** (1999) 385;  
L3 Collaboration, Phys. Lett. **B445** (1999) 428.
- [35] J. Valls, talk given at the 'XXIXth International Conference on High Energy Physics',  
Vancouver, Canada, 23-29 July 1998;  
K. De, talk given at 'SUSY 98', Keble College, Oxford, UK, 11-17 July 1998.
- [36] DØ Collaboration, preprint Fermilab-Pub-98-402-E, February 1999, [hep-ex/9902013](#).
- [37] For a recent analysis, see. e.g.:  
A. Hocker, talk presented at the DPF'99 meeting, Los Angeles, CA, 5-9 January 1999,  
preprint [hep-ex/9903024](#).
- [38] DØ Collaboration, preprint [hep-ex/9902028](#).
- [39] ATLAS Technical Proposal, CERN/LHC/94-43 LHCC/P2, December 1994.
- [40] CMS Technical Proposal, CERN/LHC/94-43 LHCC/P1, December 1994.
- [41] K. Hagiwara and D. Zeppenfeld, Nucl. Phys. **B274** (1986) 1.

## Appendix A

In this additional Section we present in analytic form the MEs adopted in calculating all our processes. We identify the external particles as follows:

$$g(p_1, \lambda_1) + g(p_2, \lambda_2) \longrightarrow \tilde{q}_\chi(p_3) + \tilde{q}_{\chi'}^*(p_4) + \Phi(p_5), \quad (\text{A.1})$$

where  $p_i$ ,  $i = 1, \dots, 5$  are the four-momenta<sup>10</sup>, and  $\lambda_j$ ,  $j = 1, 2$ , are the helicities of the QCD vector bosons.

It is convenient to rearrange the amplitudes corresponding to the graphs in Fig 1 in terms of their colour structure. For example, it is trivial to recognise the existence of only two combinations of colour matrices, namely,  $t_{ac}^A t_{cb}^B \equiv (t^A t^B)_{ab}$  and  $t_{ac}^B t_{cb}^A \equiv (t^B t^A)_{ab}$ , where  $A, B = 1, \dots, 8$  are the gluon and  $a, b, c = 1, \dots, 3$  the squark colour indices. This is immediate for graphs 1 to 6, as one can realise by explicitly writing down the QCD Feynman rules. In addition, the triple-gluon diagrams, graphs 7 and 8, are proportional to the anti-commutator  $[t^A, t^B]$ , whereas those involving quartic couplings, graphs 9 and 10, depend on the commutator  $\{t^A, t^B\}$ .

Therefore, the total amplitude of processes of the type (A.1) can be written as

$$A_{A,B;a,b}^{\{\lambda\}} = (t^A t^B)_{ab} T_1^{\{\lambda\}} + (t^B t^A)_{ab} T_2^{\{\lambda\}}. \quad (\text{A.2})$$

The two subamplitudes  $T_i^{\{\lambda\}}$ ,  $i = 1, 2$ , are obtained as follows

$$\begin{aligned} T_1^{\{\lambda\}} &= \sum_{i=1}^3 M_i^{\{\lambda\}} + \sum_{i=7}^8 M_i^{\{\lambda\}} + \sum_{i=9}^{10} M_i^{\{\lambda\}}, \\ T_2^{\{\lambda\}} &= \sum_{i=4}^6 M_i^{\{\lambda\}} - \sum_{i=7}^8 M_i^{\{\lambda\}} + \sum_{i=9}^{10} M_i^{\{\lambda\}}, \end{aligned} \quad (\text{A.3})$$

where the  $M_i^{\{\lambda\}}$ ,  $i = 1, \dots, 10$ , are the original Feynman amplitudes associated to the graphs in Fig. 1, but deprived of their colour structure (and couplings, see eq. (A.4) below)<sup>11</sup>.

This way, the total amplitude squared, summed/averaged over the final/initial spin and colours, can be expressed in terms of only two colour factors, as

$$\overline{|\mathcal{M}|^2}(gg \rightarrow \tilde{q}_\chi \tilde{q}_{\chi'}^* \Phi) = |\lambda_{\Phi \tilde{q}_\chi \tilde{q}_{\chi'}}|^2 \frac{g_s^4 g_W^2}{256} \sum_{\{\lambda\}=\pm} \sum_{i=1}^2 \sum_{j=1}^2 T_i^{\{\lambda\}} T_j^{\{\lambda\}*} C_{ij}, \quad (\text{A.4})$$

with  $g_s^2 = 4\pi\alpha_s$ ,  $g_W^2 = 4\pi\alpha_{\text{em}}/s_W^2$  and where  $C_{ij}$  is a  $(2 \times 2)$  colour matrix with elements

$$\begin{aligned} C_{11} &\equiv C_{22} = \frac{1}{4} \left( \frac{1}{N_C} - 2N_C + N_C^3 \right) = \frac{16}{3}, \\ C_{12} &\equiv C_{21} = \frac{1}{4} \left( \frac{1}{N_C} - N_C \right) = -\frac{2}{3}, \end{aligned} \quad (\text{A.5})$$

<sup>10</sup>For our purposes, we take the initial state momenta,  $p_1$  and  $p_2$ , as incoming and the final state ones,  $p_3$ ,  $p_4$  and  $p_5$ , as outgoing.

<sup>11</sup>The notation  $\{\lambda\}$  refers cumulatively to the helicities of the two incoming gluons, i.e.,  $\lambda_i$  with  $i = 1, 2$ .

as usual being  $N_C \equiv 3$  the number of colours in QCD. In eq. (A.4),  $\lambda_{\Phi_{\tilde{q}_\chi \tilde{q}'_\chi}}$  represents the strength of the squark-squark-Higgs vertex involved, as described in Sect. 3 (apart from an overall phase and the factor  $g_W$ ).

The ten amplitudes  $M_i^{\{\lambda\}}$  are simply

$$\begin{aligned}
M_1^{\{\lambda\}} &= 4\varepsilon_1(\lambda_1) \cdot p_4 \varepsilon_2(\lambda_2) \cdot (p_3 + p_5)/P_{14}/P_{35}, \\
M_2^{\{\lambda\}} &= 4\varepsilon_1(\lambda_1) \cdot (p_4 + p_5) \varepsilon_2(\lambda_2) \cdot p_3/P_{23}/P_{45}, \\
M_3^{\{\lambda\}} &= 4\varepsilon_1(\lambda_1) \cdot p_4 \varepsilon_2(\lambda_2) \cdot p_3/P_{14}/P_{23}, \\
M_4^{\{\lambda\}} &= 4\varepsilon_1(\lambda_1) \cdot (p_3 + p_5) \varepsilon_2(\lambda_2) \cdot p_4/P_{24}/P_{35}, \\
M_5^{\{\lambda\}} &= 4\varepsilon_1(\lambda_1) \cdot p_3 \varepsilon_2(\lambda_2) \cdot (p_4 + p_5)/P_{13}/P_{45}, \\
M_6^{\{\lambda\}} &= 4\varepsilon_1(\lambda_1) \cdot p_3 \varepsilon_2(\lambda_2) \cdot p_4/P_{24}/P_{13}, \\
M_7^{\{\lambda\}} &= \varepsilon_{12}(\lambda_1, \lambda_2) \cdot (-2p_4 + p_1 + p_2)/P_{35}, \\
M_8^{\{\lambda\}} &= \varepsilon_{12}(\lambda_1, \lambda_2) \cdot (+2p_3 - p_1 - p_2)/P_{45}, \\
M_9^{\{\lambda\}} &= \varepsilon_1(\lambda_1) \cdot \varepsilon_2(\lambda_2)/P_{35}, \\
M_{10}^{\{\lambda\}} &= \varepsilon_1(\lambda_1) \cdot \varepsilon_2(\lambda_2)/P_{45},
\end{aligned} \tag{A.6}$$

where we have introduced the propagator functions

$$\begin{aligned}
P_{14} &= (p_1 - p_4)^2 - M_{\tilde{q}'_\chi}^2, \\
P_{24} &= (p_2 - p_4)^2 - M_{\tilde{q}'_\chi}^2, \\
P_{23} &= (p_2 - p_3)^2 - M_{\tilde{q}_\chi}^2, \\
P_{13} &= (p_1 - p_3)^2 - M_{\tilde{q}_\chi}^2, \\
P_{35} &= (p_3 + p_5)^2 - M_{\tilde{q}'_\chi}^2 + iM_{\tilde{q}'_\chi} \Gamma_{\tilde{q}'_\chi}, \\
P_{45} &= (p_4 + p_5)^2 - M_{\tilde{q}_\chi}^2 + iM_{\tilde{q}_\chi} \Gamma_{\tilde{q}_\chi},
\end{aligned} \tag{A.7}$$

the gluon polarisation vectors [41],  $i = 1, 2$ ,

$$\begin{aligned}
\varepsilon_i^\mu(\lambda_i = \pm) &= \frac{1}{\sqrt{2}}[\mp \varepsilon_i^\mu(\lambda_i = 1) - i \varepsilon_i^\mu(\lambda_i = 2)], \\
\varepsilon_i^\mu(\lambda_i = 1) &= (|\vec{p}_i| p_i^T)^{-1} (0, p_i^x p_i^z, p_i^y p_i^z, -p_i^{T^2}), \\
\varepsilon_i^\mu(\lambda_i = 2) &= (p_i^T)^{-1} (0, -p_i^y, p_i^x, 0),
\end{aligned} \tag{A.8}$$

with

$$\begin{aligned}
p_i^T &= \sqrt{p_i^{x^2} + p_i^{y^2}}, \\
|\vec{p}_i| &= \sqrt{p_i^{x^2} + p_i^{y^2} + p_i^{z^2}},
\end{aligned} \tag{A.9}$$

and their contraction over the triple-gluon vertex times the gluon propagator

$$\begin{aligned}\varepsilon_{12}^\mu(\lambda_1, \lambda_2) = & \frac{1}{P_{12}} \{ (p_1 - p_2)^\mu \varepsilon_1(\lambda_1) \cdot \varepsilon_2(\lambda_2) \\ & + [(p_2 + p_{12}) \cdot \varepsilon_1(\lambda_1)] \varepsilon_2^\mu(\lambda_2) - [(p_1 + p_{12}) \cdot \varepsilon_2(\lambda_2)] \varepsilon_1^\mu(\lambda_1) \},\end{aligned}\tag{A.10}$$

with  $P_{12} = p_{12}^2 \equiv (p_1 + p_2)^2$ .



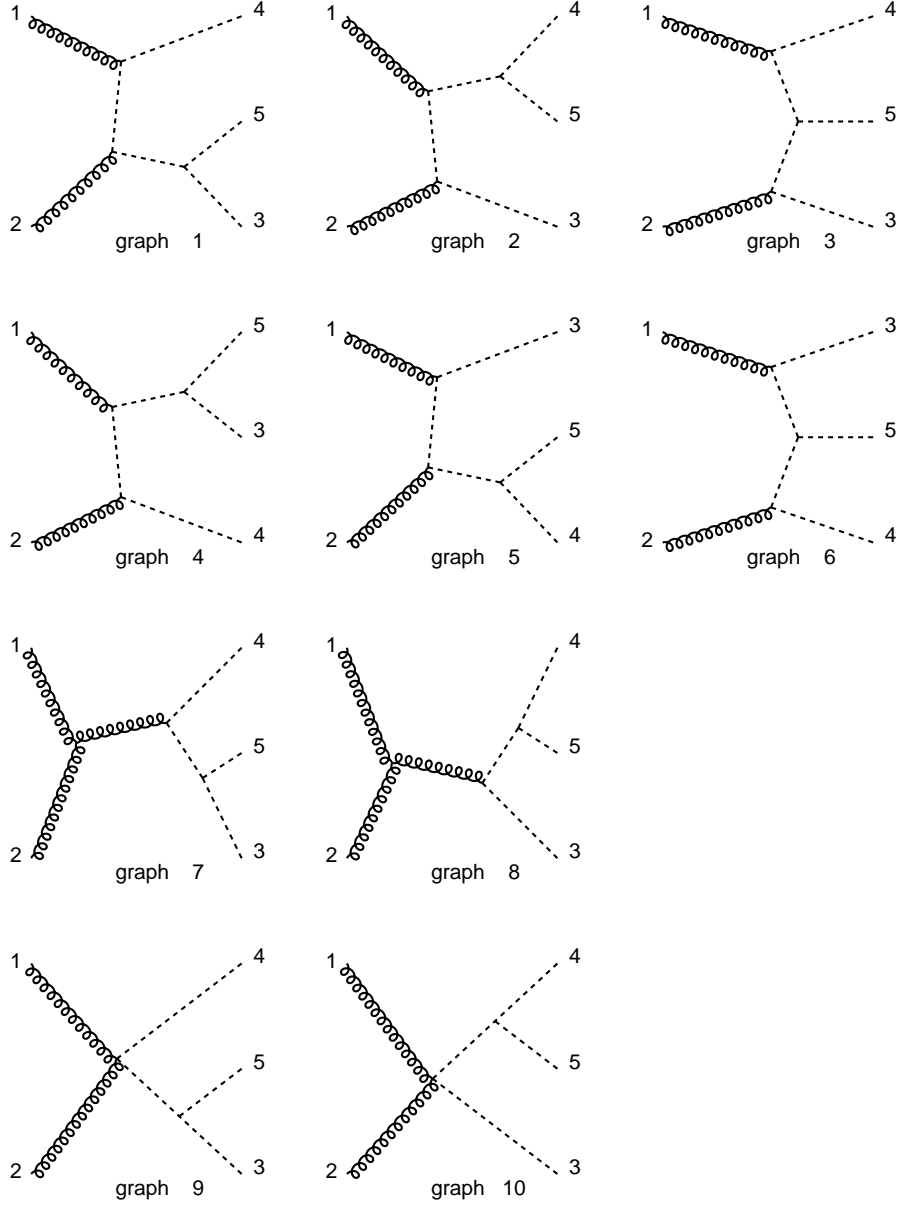


Figure 1: Feynman diagrams contributing at lowest order to processes (A.1). An helical line refers to a gluon whereas a dashed one symbolises both a squark and a Higgs boson.

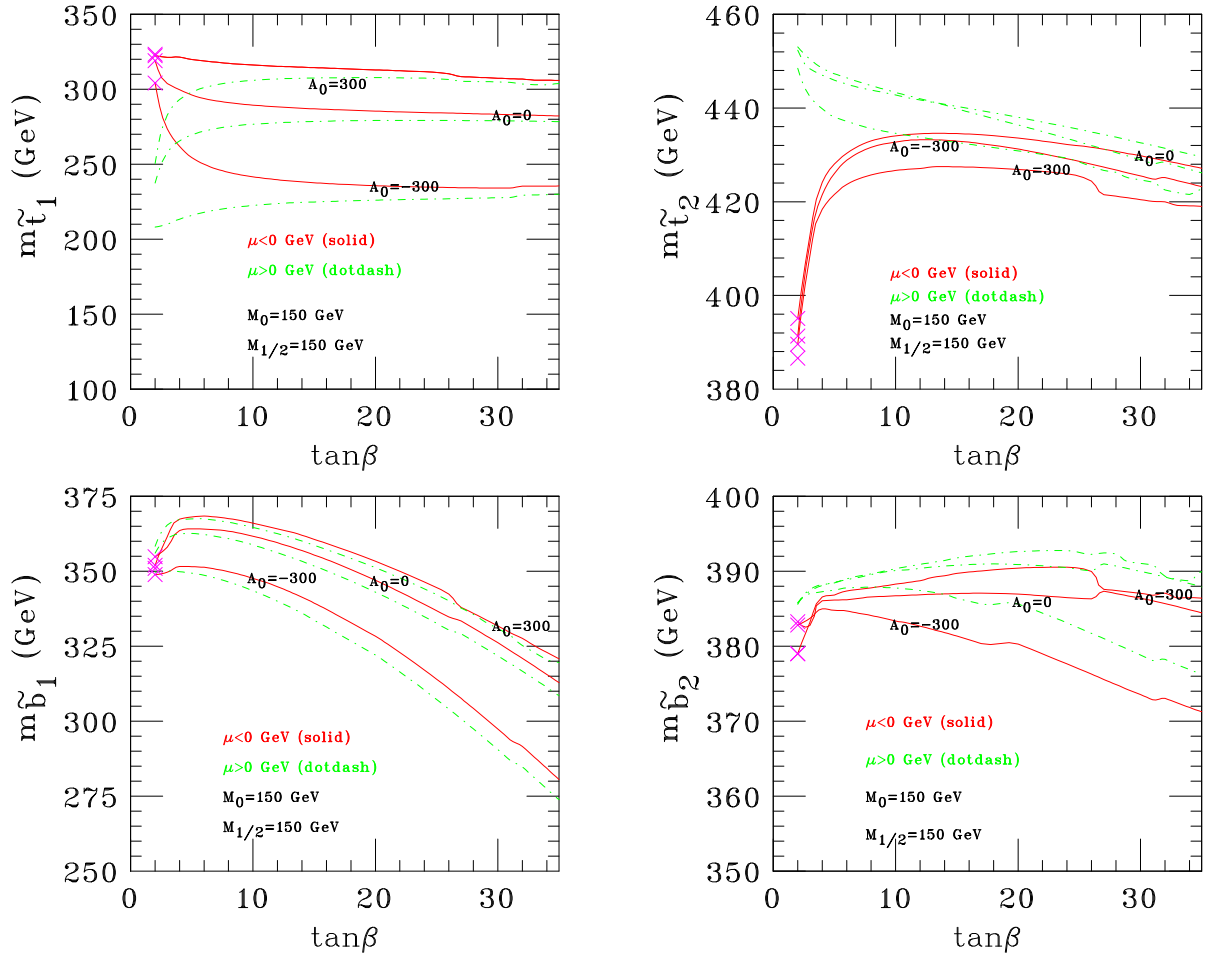


Figure 2: Resulting masses from [10] for the third generation of squarks versus  $\tan\beta$  for three values of  $A_0$  and for both positive (dot-dashed) and negative (solid)  $\mu$ .

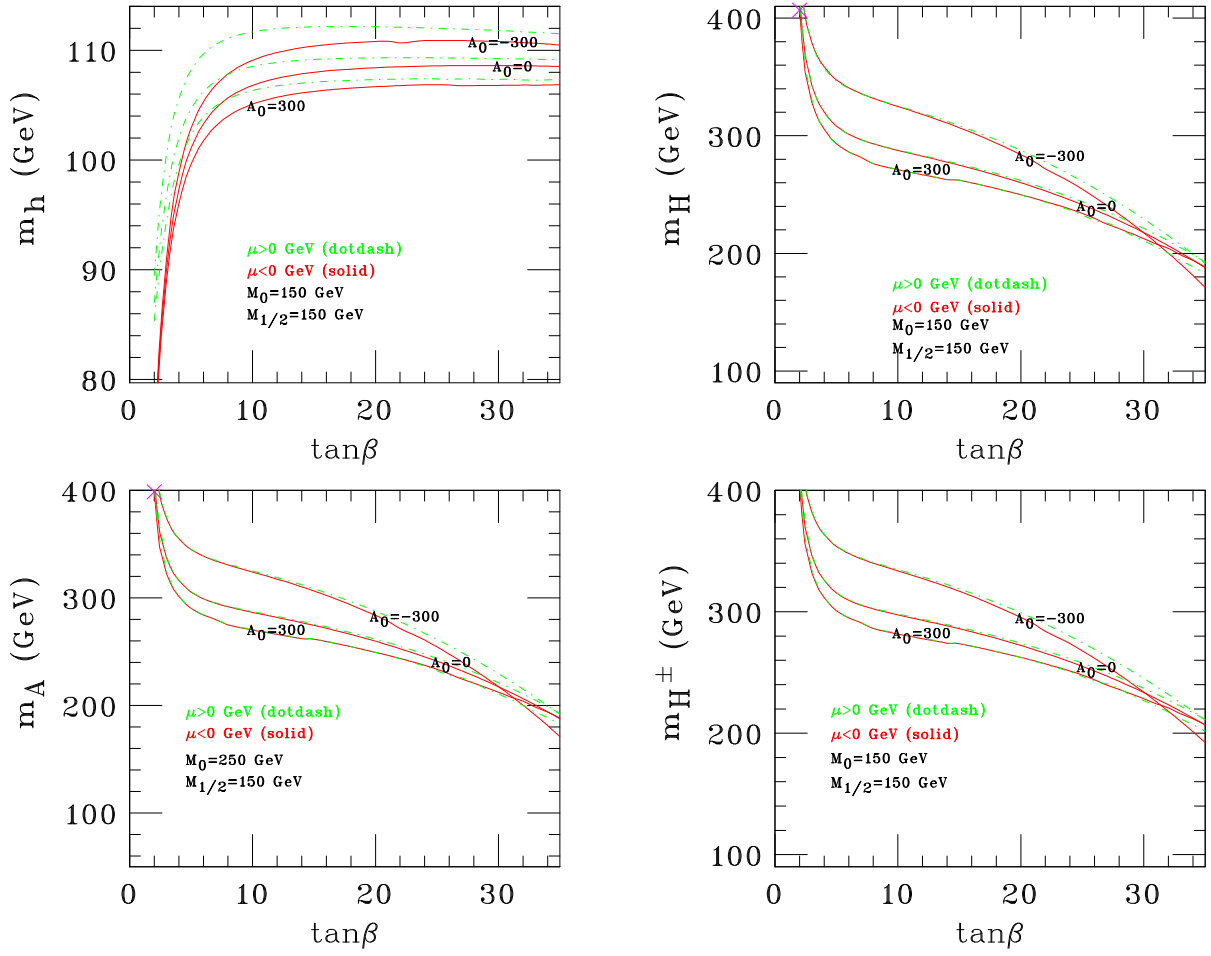


Figure 3: Resulting masses from [10] for the five Higgs bosons versus  $\tan\beta$  for three values of  $A_0$  and for both positive (dot-dashed) and negative (solid)  $\mu$ .

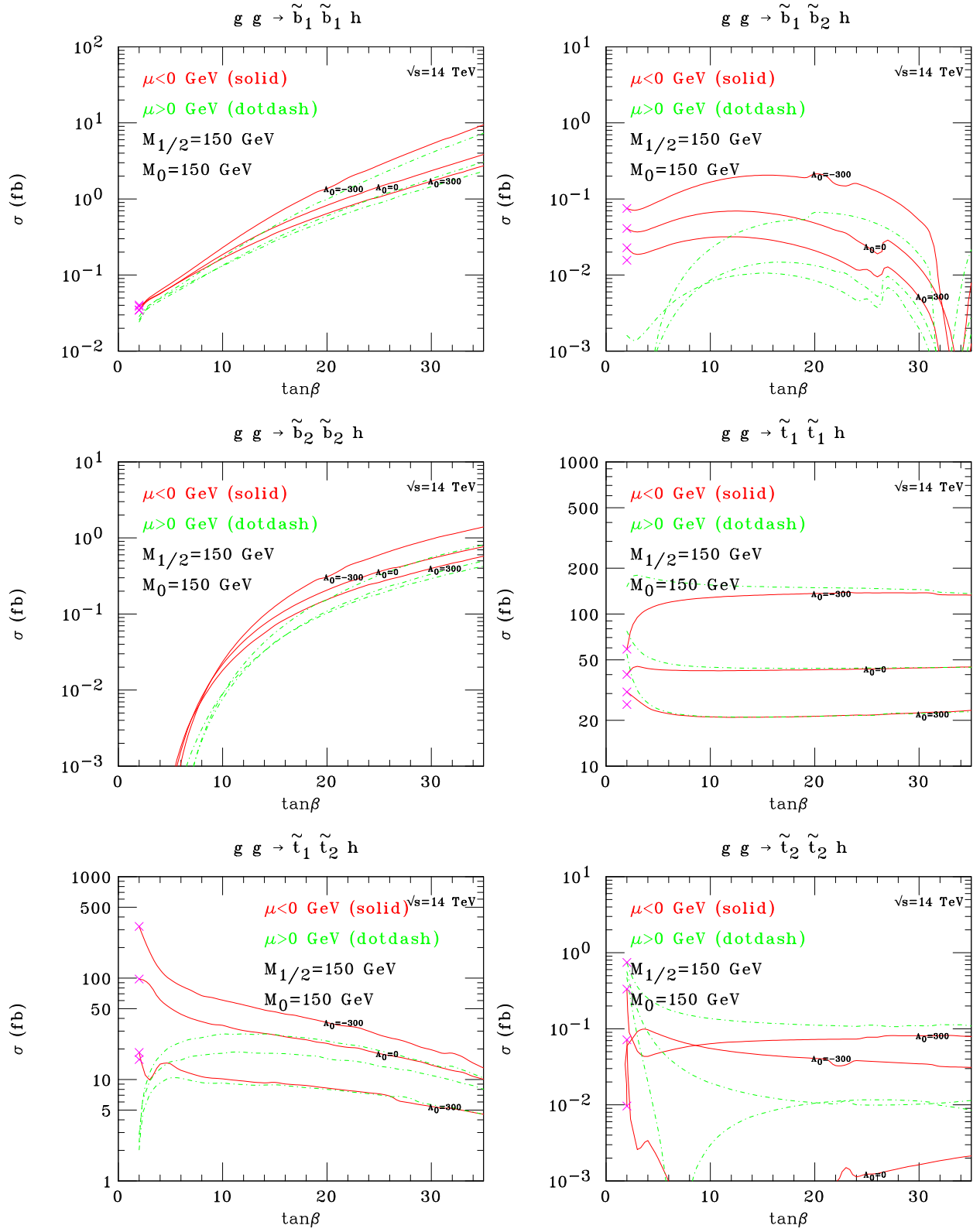


Figure 4: Total cross section of  $gg \rightarrow \tilde{q}_{1,2}\tilde{q}_{1,2}h$  processes (with  $q = t, b$ ) as a function of  $\tan\beta$  for the characteristic input values  $M_0 = 150$  GeV and  $M_{1/2} = 150$  GeV. Both positive (dot-dashed) and negative (solid)  $\mu$  as well as several  $A_0$  contour lines are shown. The symbol “x” is used to indicate parameter areas forbidden by direct Higgs boson searches.

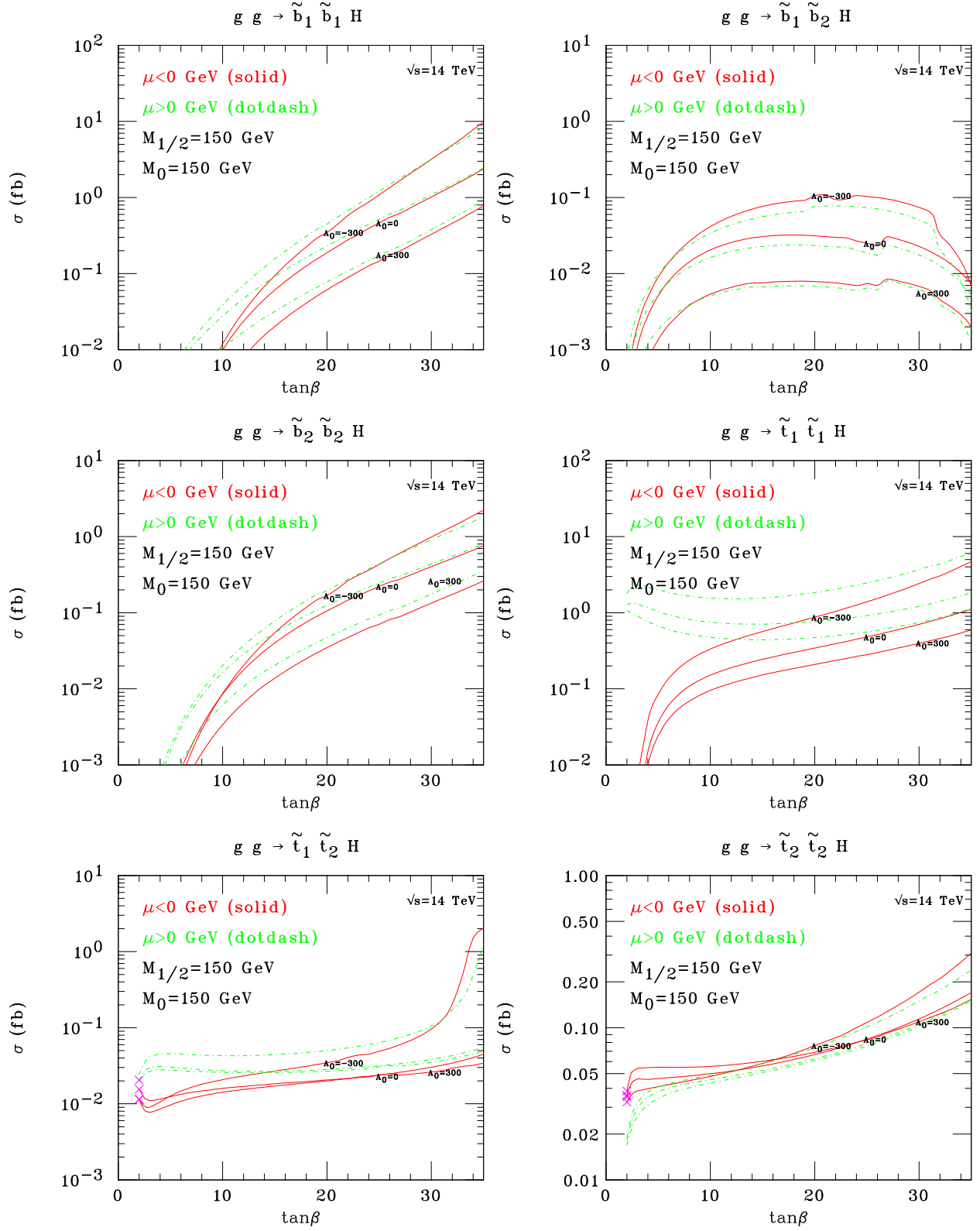


Figure 5: Total cross section of  $gg \rightarrow \tilde{q}_{1,2}\tilde{q}_{1,2}H$  processes (with  $q = t, b$ ) as a function of  $\tan\beta$  for the characteristic input values  $M_0 = 150$  GeV and  $M_{1/2} = 150$  GeV. Both positive (dot-dashed) and negative (solid)  $\mu$  as well as several  $A_0$  contour lines are shown. The symbol “ $\times$ ” is used to indicate parameter areas forbidden by direct Higgs boson searches.

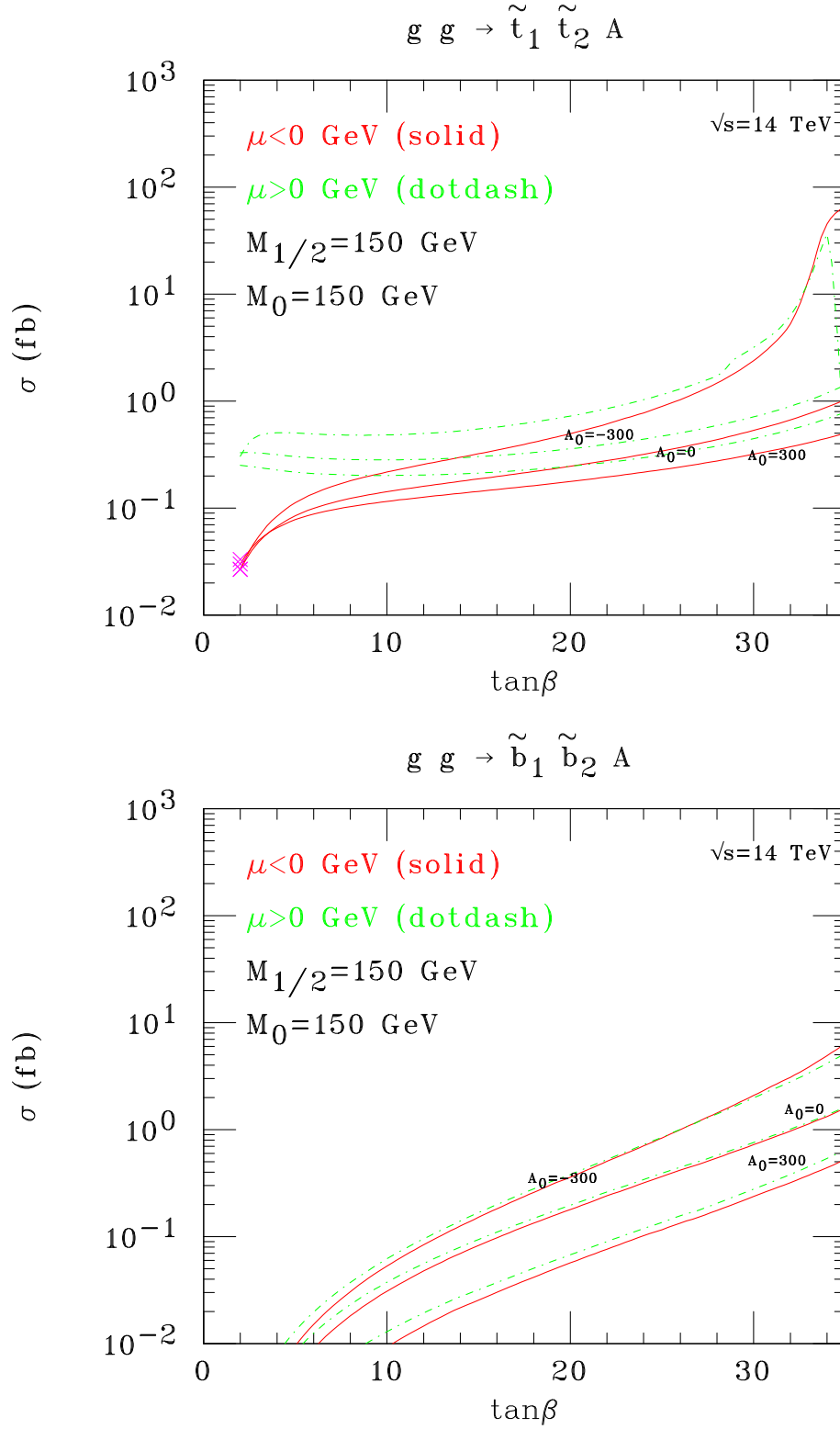


Figure 6: Total cross section of  $gg \rightarrow \tilde{q}_1 \tilde{q}_2 A$  processes (with  $q = t, b$ ) as a function of  $\tan\beta$  for the characteristic input values  $M_0 = 150$  GeV and  $M_{1/2} = 150$  GeV. Both positive (dot-dashed) and negative (solid)  $\mu$  as well several  $A_0$  contour lines are shown. The symbol “ $\times$ ” is used to indicate parameter areas forbidden by direct Higgs boson searches.

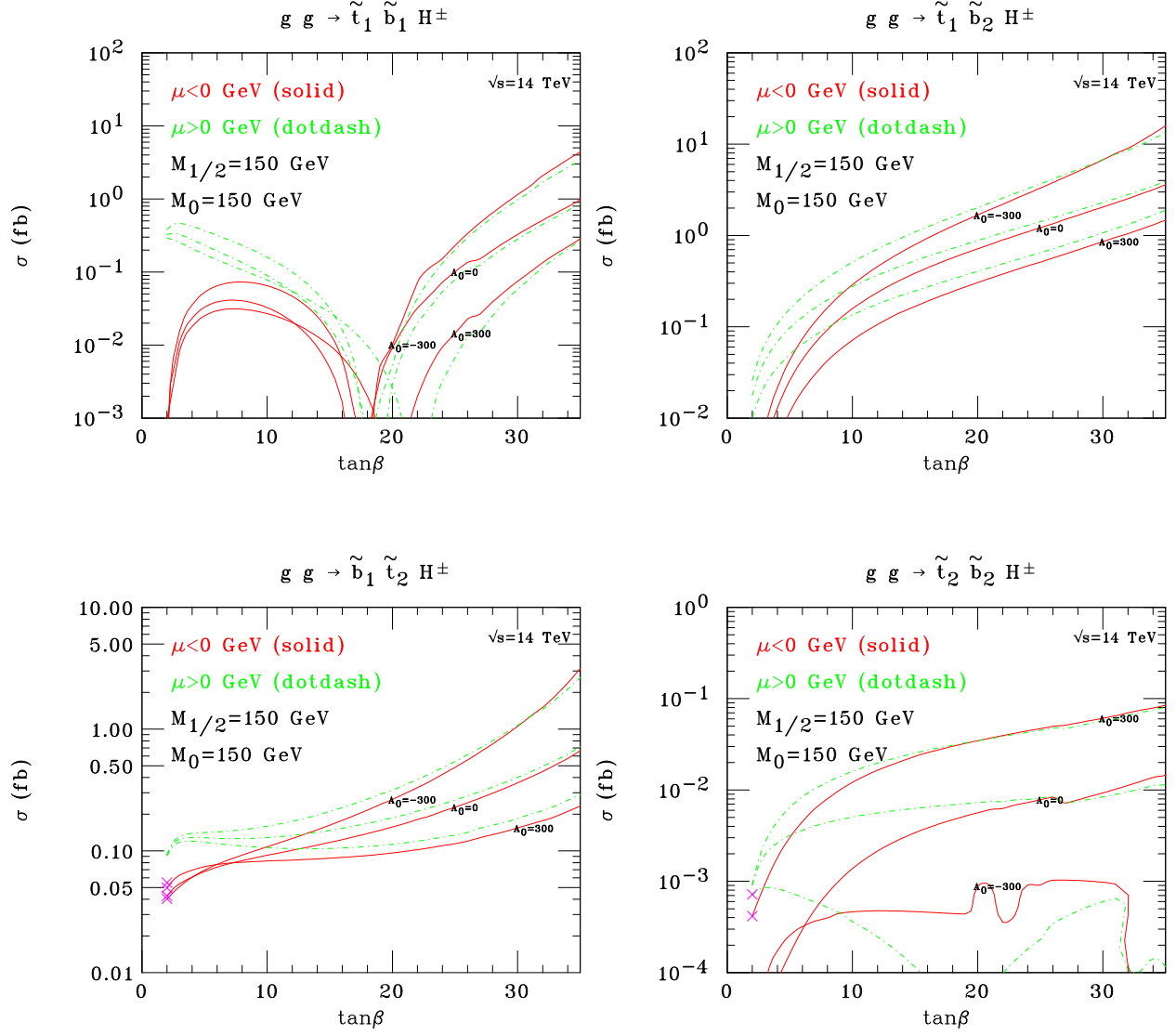


Figure 7: Total cross section of  $gg \rightarrow \tilde{q}_{1,2} \tilde{q}'_{1,2} H^\pm$  processes (with  $q^{(\prime)} = t, b$ ) as a function of  $\tan\beta$  for the characteristic input values  $M_0 = 150$  GeV and  $M_{1/2} = 150$  GeV. Both positive (dot-dashed) and negative (solid)  $\mu$  as well as several  $A_0$  contour lines are shown. The symbol "×" is used to indicate parameter areas forbidden by direct Higgs boson searches.

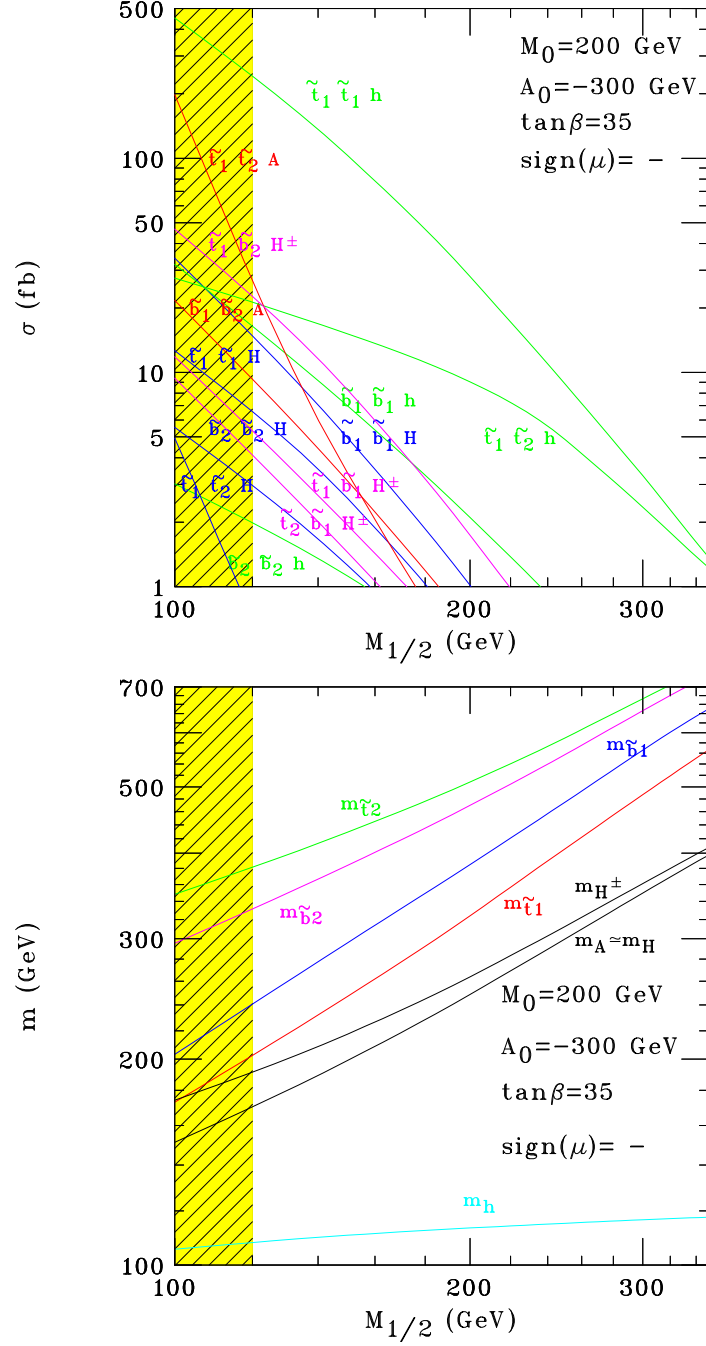


Figure 8: The most significant cross sections which survive the choice of a light SUSY spectrum (above), alongside the values for the masses entering the corresponding production processes (below). Shaded regions indicate areas excluded by direct searches.



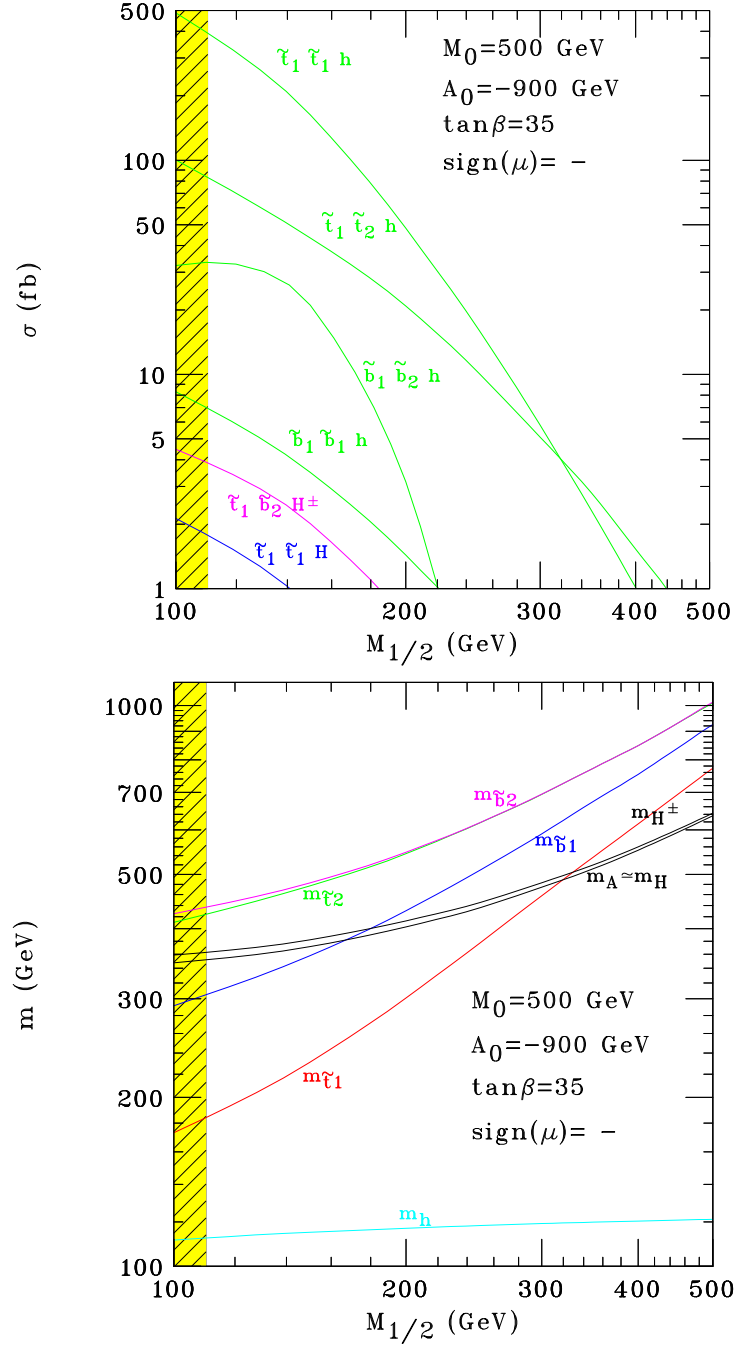


Figure 9: The most significant cross sections which survive the choice of a heavy SUSY spectrum (above), alongside the values for the masses entering the corresponding production processes (below). Shaded regions indicate areas excluded by direct searches.